https://doi.org/10.5194/egusphere-2025-117
Preprint. Discussion started: 20 February 2025

The influence of a rock glacier on the riverbed hydrological system

Bastien Charonnat[1,6,7], Michel Baraer[1,6,7], Eole Valence[2,6], Janie Masse-Dufresne[1,6,7], Chloé Monty[3], Kaiyuan Wang[4], Elise Devoie[5], Jeffrey M. McKenzie[2]

[1]Hydrology, Climate and Climate Change laboratory – École de technologie supérieure (ÉTS), Montreal, Quebec, Canada
[2] Department of Earth and Planetary Science – McGill University, Montreal, Quebec, Canada
[3] Department of Earth Sciences – Simon Fraser University, Burnaby, British Columbia, Canada
[4] Department of Earth, Environmental & Planetary Sciences – Brown University, Providence, Rhode Island, United States
[5] Civil Engineering department – Queen's University, Kingston, Ontario, Canada
[6] GEOTOP (Research Centre on the Dynamics of the Earth System), Montreal, Quebec, Canada
[7] CentrEau (Quebec Research Water Centre), Quebec City, Quebec, Canada

Correspondence to: Bastien Charonnat (bastien.charonnat.1@ens.etsmtl.ca)

Abstract

Climate change is accelerating cryosphere degradation in mountainous regions, altering hydrological and geomorphological dynamics in deglaciating catchments. Among cryospheric features, rock glaciers degrade more slowly than glaciers, providing a sustained influence on water resources in alpine watersheds. This study investigates the role of a rock glacier interacting with the Shár Shaw Tagà River (Grizzly Creek) riverbed in the St. Elias Mountains (Yukon, Canada), using a unique multimethod approach that integrates hydro-physicochemical and isotopic characterization, drone-based thermal infrared (TIR) imagery, and visible time-lapse (TL) imagery. Results assess that rock glaciers, due to their geomorphic properties, can constrict riverbeds and alluvial aquifers, and control shallow groundwater flow, leading to notable changes in channel structure and groundwater discharge. These disruptions promote downstream cryo-hydrological processes by facilitating aufeis formation and modifying the physicochemical properties of streamflow. Additional findings highlight the critical role of rock glaciers and proglacial systems in connecting mountain cryosphere and deep groundwater systems, with consequent implications for mountain hydrology and water resources.

1. Introduction

Climate change is profoundly transforming mountain regions, where the cryosphere plays a critical role in regulating water resources essential for the sustainability of downstream ecosystems and communities. With rising global temperatures, high mountain areas are experiencing accelerated deglaciation, characterized by glacial retreat and permafrost thaw (Hock et al., 2019). These processes drive rapid geomorphological and hydrological reconfigurations in proglacial systems (Carrivick and Heckmann, 2017). Understanding the impacts of cryosphere degradation on mountain hydrology and hydrogeology is essential

https://doi.org/10.5194/egusphere-2025-117
Preprint. Discussion started: 20 February 2025

for predicting future water availability in these regions. Recently, the connectivity between the cryosphere and groundwater has been identified as a critical issue in mountain hydrology, directly influencing water resource sustainability under changing climatic conditions (van Tiel et al., 2024).

In proglacial systems, riverbeds and outwash plains serve as critical hydrogeological components, sustaining baseflow and aquatic habitats (Käser and Hunkeler, 2016; Müller et al., 2024). However, the recharge and discharge dynamics of alluvial groundwater systems are intrinsically linked to upstream and adjacent cryospheric features (e.g., glaciers, seasonal snowpacks, etc.; Müller et al., 2024), as evidenced by aufeis formation. Aufeis, or icings, are layered ice formations that develop in winter when groundwater outflows persist under sub-zero temperatures for several months (Ensom et al., 2020). These formations can occur due to upwellings of groundwater encountering impermeable permafrost (Terry et al., 2020), with channel constriction further promoting their formation (Wainstein et al., 2014; Liu et al., 2021). In mountain environments, aufeis formations are common in outwash plains and are generally supplied by groundwater and meltwater from surrounding cryospheric sources (Chesnokova et al., 2020; Mallinson et al., 2019; Wainstein et al., 2014).

Among cryospheric features, rock glaciers degrade more slowly than glaciers, allowing them to exert a prolonged influence on hydrological processes as glaciers retreat (Bolch and Marchenko, 2009; Harrison et al., 2021; Jones et al., 2021). Despite growing recognition of their hydrological importance, rock glaciers remain understudied compared to glaciers, particularly concerning their roles in deglaciating catchments (Jones et al., 2019). Rock glaciers are tongue-shaped landforms composed of rocky debris and ice, which creep due to the plastic deformation of their frozen content. They are commonly found in high mountain environments and occur in both discontinuous and continuous permafrost zones (Barsch, 1996). While existing studies primarily focus on the internal hydrological behavior of rock glaciers, research addressing their broader catchment-scale implications remains limited (Jones et al., 2019).

Rock glaciers have been shown to buffer surface waters throughout the year, sustaining baseflow during dry periods and attenuating discharge response to intense precipitation events due to their internal structure (Bearzot et al., 2023; Reato et al., 2022; Wagner et al., 2021). Their hydrological behaviour is closely tied to the distribution of frozen and liquid water within them (Harrington et al., 2018; Wagner et al., 2016; Winkler et al., 2016). Unfrozen layers in summer can act as reservoirs and conduits for water flow (Halla et al., 2021; Harrington et al., 2018; Navarro et al., 2023; Wagner et al., 2020). In addition to liquid water, intact rock glaciers (i.e., containing frozen content) store significant volumes of solid water as interstitial or massive ice (Chakravarthi et al., 2022; Halla et al., 2021; Jones et al., 2018; Wagner et al., 2021). However, internal ice melt typically contributes only minimally to total rock glacier discharge (Arenson et al., 2022). In addition to modulating discharge, rock glaciers influence downstream water quality by increasing solute concentrations (Colombo et al., 2018; Colombo et al., 2019; Schreder et al., 2023; Engel et al., 2019; Wanner et al., 2023; Zarroca et al., 2021) and cooling stream temperatures (Bearzot et al., 2023; Brighenti et al., 2019; Colombo et al., 2020). The physicochemical impact of rock glacier outflows is particularly pronounced at the catchment scale when compared to catchments lacking glacial or periglacial landforms (Brighenti et al., 2023; Clow et al., 2021; Del Siro et al., 2023; Gammons et al., 2021; Robinson et al., 2022).

https://doi.org/10.5194/egusphere-2025-117
Preprint. Discussion started: 20 February 2025

While much of the literature focuses on the downstream effects of rock glacier outflows (e.g., Brighenti et al., 2023; Robinson et al., 2022; Wagner et al., 2016; Wagner et al., 2021), their influence on the hydrogeomorphology of riverbeds and outwash plains remains understudied. Rock glaciers can advance, constrain, and dam riverbeds, potentially forming ponds, as reported in High Asia (Blöthe et al., 2019; Falatkova et al., 2020; Hewitt, 2014) and the Alps (Colombo et al., 2020). Furthermore, topographic changes driven by glacial retreat and paraglacial processes can force channel confinement (Marren and Toomath, 2014). Climate change has intensified rock glacier movement (Delaloye et al., 2010; Kummert et al., 2019; PERMOS, 2019), sometimes causing destabilization (Marcer et al., 2021) and channel disruption (Sorg et al., 2015). Additionally, sudden mass movements, such as the catastrophic collapse of rock glacier lobes, have triggered debris flows with downstream geomorphic impacts (Bodin et al., 2015; Scotti et al., 2017). The hydrological and geomorphic disturbances caused by advancing rock glaciers in valley systems are particularly notable, given the critical role of riverbeds and outwash plains in sustaining water resources. Despite recent studies (e.g., Falatkova et al., 2020; Wagner et al., 2021), research on the interactions between rock glaciers, the adjacent cryosphere, surface waters, and groundwater flow within valley systems is still underexplored.

This study investigates the influence of rock glaciers on surface and shallow groundwater flow within riverbed hydrological systems. Specifically, it examines the critical impact of a rock glacier in the Shár Shaw Tagà catchment (St. Elias Mountains, Yukon, Canada) on the watershed's hydrological dynamics. The study's originality lies in its focus on the indirect effects of the rock glacier on the riverbed hydrological system, even in the absence of a prominent visible outflow. By providing insights into the hydrological, hydrogeological, and physicochemical processes associated with rock glaciers, this research offers findings that are globally applicable. A multimethod approach is employed, combining hydro-physicochemical and isotopic characterization, with synoptic sampling, drone-based thermal infrared (TIR) imagery, and visible time-lapse (TL) imagery.

2. Study site

Shár Shaw Tagà, meaning Grizzly Creek in the Southern Tutchone indigenous language, is a 32 km² glacierized catchment located within the traditional lands of the Kluane First Nation and the White River First Nation. It also lies within the boundaries of Kluane National Park and Reserve in the St. Elias Mountains, southwestern Yukon Territory, Canada (61°05'12.6" N, 139°07'17.6" W). The eastern flank of the St. Elias Mountains experiences a dry subarctic climate, with annual precipitation ranging from 300 to 500 mm yr^{-1} (Wahl et al., 1987).

The upper Shár Shaw Tagà catchment (Fig. 1b) contains eight glaciers, the largest of which is G-A1, covering an area of 3.2 km². Faults are inferred along the valley floor (Dodds and Campbell, 1992). Due to its heavily fractured bedrock lithology and steep slopes, the valley is characterized by significant mass wasting processes and depositional features, including nine previously identified rock glaciers (Johnson, 1978; Evin et al., 1997). Between 1974 and 1997, Johnson participated to a series of geomorphological studies on the valley (Johnson, 1974; 1978; 1980; 1983; 1986; 1992; Evin et al., 1997), providing detailed descriptions of its landforms. The geomorphological identification and landform naming for these features, as established in Johnson's works, are adopted in this study to characterize the geomorphological setting.

https://doi.org/10.5194/egusphere-2025-117
Preprint. Discussion started: 20 February 2025

The significance of ground ice landforms in the valley has prompted recent investigations, including a study on buried ice detection using ground-penetrating radar (GPR) in rocky and steep terrains (Tjoelker et al., 2024). Publications prior to 2024 referred to the area by the toponym "Grizzly Creek" rather than Shár Shaw Tagà. Of the nine rock glaciers identified by Johnson and Evin et al. (1978; 1997), seven extend into the riverbed along the valley floor, with some exerting considerable geomorphological constraints on the stream.

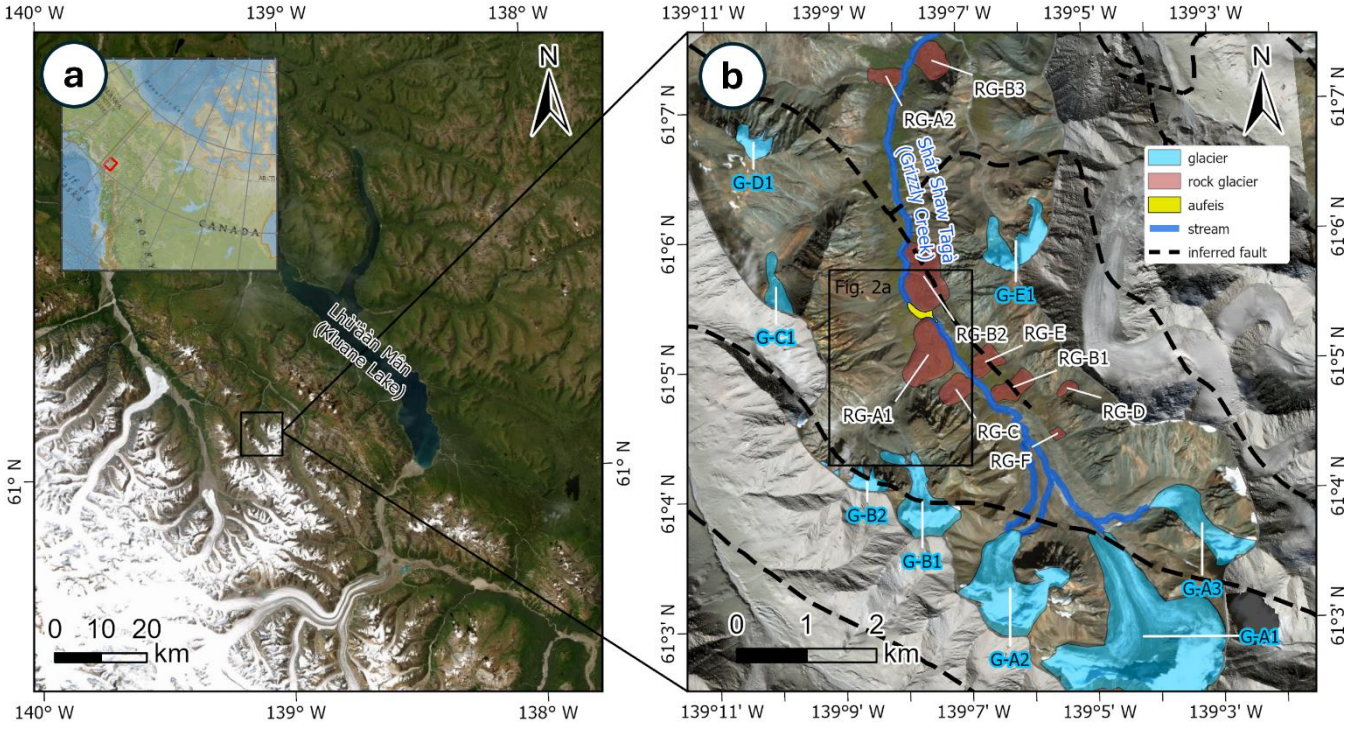

Fig. 1: (a) Overview map showing the location of the Shár Shaw Tagà valley in southwestern Yukon, Canada. (b) Enlarged view of the study area from panel (a), highlighting key geomorphological features. The black frame outlines the extent of the map shown in Fig. 2b. Rock glaciers identified in earlier studies (Johnson, 1978; Evin et al., 1997) are marked in red. The study focuses on the RG-A1 rock glacier, located at the confluence of the G-A1 and G-B1 subcatchments. The Shár Shaw Tagà River, fed by glaciers G-A1, G-A2, and G-A3, is constrained against the opposite talus slope by the RG-A1 rock glacier. An aufeis formation, highlighted in yellow, develops during winter on the outwash plain between RG-A1 and RG-B2. The fault network inferred by Dodds and Campbell (1992) reveals the area's fractured bedrock and faulted geology. ArcticDEM data: Polar Geospatial Center (Porter et al., 2023). Basemap credits: Esri.

The present study investigates the hydrological influence of the RG-A1 rock glacier, located on the western side of the upper Shár Shaw Tagà valley. RG-A1, first identified by Johnson (1978), spans elevations between 1700 and 1850 m a.s.l. The southern lobes of RG-A1 appear older, characterized by vegetation cover and a smoother frontal morphology, while the northern lobes are younger, with sparse or absent vegetation, sharper forms, and a steeper front (Johnson, 1978). A frozen layer, 20 to 40 m thick was detected in RG-A1 during a previous geophysical study, which also suggested the presence of massive ice lenses at depth (Evin et al., 1997). The front of RG-A1 advances in the valley, constraining the Shár Shaw Tagà

https://doi.org/10.5194/egusphere-2025-117
Preprint. Discussion started: 20 February 2025

River against the opposing talus slope. Although previous studies did not classify the opposing talus slope as a rock glacier, it is suspected to be a protalus rampart (or small active rock glacier) based on environmental and topographic criteria outlined in Scapozza (2015), such as the absence of an upstream permanent snow field, the presence of coarse boulders in the upslope area, a steep front with exposed fine sediments, and its juxtaposition and superimposition to other rock glaciers.

The outwash plains upstream and downstream of RG-A1 are separated by a "narrow section" of the Shár Shaw Tagà River, which can be divided into two subsections: N1 and N2. N1 extends from the outlet of the upstream outwash plain to a bedrock outcrop visible on the opposite talus slope to RG-A1. N2 extends from this bedrock outcrop to the outlet of the "narrow section", where the rivers enters the downstream outwash plain. An aufeis forms in winter in the downstream outwash plain, as confirmed through field studies since 2018 and satellite imagery. No aufeis has been detected in the upstream outwash plain during this period.

In 1974, Johnson (1978) observed that meltwater drained into a sinkhole located in the rooting zone of RG-A1 (at approximately 1850 m a.s.l.), with no major resurgence observed at the front (at 1700 m a.s.l.). In 1975, a new sinkhole was observed upstream of the first one, and a significant resurgence was reported on the northern part of RG-A1. Dry channels on the surface of RG-A1 in 1975 were interpreted by Johnson as abandoned surface drainage pathways, highlighting the dynamic and variable hydrological behaviour of RG-A1.

Field observations by our research team from 2018 to 2023 confirm the absence of a significant visible outlet from the rock glacier, despite its location downstream of a 8 km^2 subcatchment, consisting of the G-B1 and G-B2 glaciers. The only visible outlets consist of low-discharge springs around the RG-A1 front, particularly concentrated along the N1 subsection. During low-discharge periods such as June 2023, we observed that the water from the Shár Shaw Tagà River infiltrates the riverbed, leaving it dry before entering the outwash plain upstream of RG-A1. However, water was observed to flow again within the riverbed in the N1 subsection, visually sustained by springs and seepage. During high-flow periods, the springs emerge directly under the front of RG-A1. In dry periods, like June 2023, the springs shift away from the front and align with the current river level, 10 to 20 m downstream.

3. Methods

3.1 Method overview

Since 2018, we have been investigating the hydrological and hydrochemical influence of RG-A1 on the Shár Shaw Tagà catchment using a multimethod approach. Our primary hypothesis posits that RG-A1 influences the formation of aufeis in the downstream outwash plain. To test this hypothesis, we monitored aufeis formation and winter outflows by deploying a timelapse (TL) camera in 2018, followed by a second TL camera installation in 2019. Additionally, an inventory of springs was conducted in 2018, 2019 and 2021. These initial observations provided a preliminary understanding of the location and timing of cryo-hydrological processes in the vicinity of RG-A1.

https://doi.org/10.5194/egusphere-2025-117
Preprint. Discussion started: 20 February 2025

Given the position of RG-A1 at the outlet of G-B1 subcatchment and the absence of significant surface outflow from it, we hypothesized that the rock glacier drains the G-B1 subcatchment, and contributes to river discharge through groundwater exfiltration. To investigate this, we sampled the Shár Shaw Tagà River and springs near RG-A1 in 2022 and 2023 to analyze their physicochemical properties. Sampling was extended to the entire subcatchment upstream of RG-A1, including the ice-debris complex and the G-B1 glacier snout, to identify potential water sources contributing to RG-A1's groundwater outflow. The aim of this analysis was to elucidate the origins of the spring waters and assess their hydrochemical impact on the Shár Shaw Tagà River.

The final phase of the study focused on characterizing the extent and magnitude of groundwater-surface interactions underlined by the spring inventory and hydrochemical analysis. Due to the large spatial scale (several hundred meters) and the challenges associated with differential stream gauging in proglacial environments, stream temperature heterogeneity was selected as a proxy for detecting groundwater exfiltration (Baker et al., 2018; Brunner et al., 2017; Kalbus et al., 2006; Webb et al., 2008). To this end, a drone-based thermal infrared (TIR) survey was conducted in June 2024 to identify zones of groundwater exfiltration. This survey provided a detailed map of preferential groundwater exfiltration locations, contributing to the overall understanding of the rock glacier's influence on the riverbed hydrologic system.

3.2 TL monitoring

Two RGB timelapse (TL) cameras, designated TL1 and TL2, were positioned above the right bank of the Shár Shaw Tagà River (Fig. 2). TL1 was installed in 2018, focused on the central area of the outwash plain immediately downstream of RG-A1. In 2019, TL2 was added adjacent to TL1, extending its field of view from the upper margin of TL1's coverage to the outlet of the N2 subsection of the Shár Shaw Tagà River. Both cameras were configured to capture four images daily at 8:00, 11:00, 13:00, and 16:00. The visual analysis of the images captured by the TL cameras involved identifying signs of surface overflow on the developing aufeis and documenting the occurrence of such events throughout the winter, following the protocol outlined by Chesnokova et al. (2020).

3.3 Physico-hydrochemical characterisation

3.3.1 Sampling and field measurements

Physico-hydrochemical characterisation was undertaken over three distinct campaigns: June 2022, August 2022, and June 2023. These campaigns targeted both the Shár Shaw Tagà River and springs inventoried from 2018 to 2021, capturing different hydrological conditions. The June 2022 campaign coincided with the melt of a late and substantial snowpack. The August 2022 campaign took place during late summer, when glacial ablation was at its peak. The June 2023 campaign was conducted following a winter with reduced snowpack and early snowmelt, after the primary snowmelt phase but before summer glacial ablation commenced, while glaciers remained snow-covered.

https://doi.org/10.5194/egusphere-2025-117
Preprint. Discussion started: 20 February 2025

Field measurements included in situ pH, electrical conductivity (EC, corrected to 25 °C, expressed in µS cm^{-1}), and water temperature (°C). Water samples were collected for laboratory analyses. Additionally, in June 2023, in situ radon measurements were performed to further investigate groundwater contributions. Measurements were taken at each sampling site using a calibrated Hanna HI 98195 multiparameter meter.

Water sampling followed a synoptic approach for cycles of 1-2 days, avoiding precipitation periods (e.g. Baraer et al., 2009). When possible, sites were sampled multiple times within each campaign to account for diurnal fluctuations in physicochemical parameters. Samples were categorized into four types (Table S1): glacial outlets from the RG-B1 snout (S-GL#), streams in the ice-debris complex located between the RG-B1 snout and RG-A1 (S-IDC#), springs at the RG-A1 front and opposite talus (S-RG#), and Shár Shaw Tagà River (S-R#). Water samples were filtered using 0.45 µm syringe filters and collected in 50 mL HDPE bottles, rinsed three times prior to sampling. Not all sites were accessible during each campaign (Table S1), due to factors such as no flow or safety concerns related to snow cover and rockfalls.

Results were analyzed following the methodology of Baraer et al. (2015). Samples for major ion analysis were stored in a dark environment at 4 °C until analysis. Major ions (Ca^{2+}, Mg^{2+}, Na^{+}, Cl^{-}, SO_4^{2-}) and minor ions (K^{+}, F^{-}) were analyzed at the LG2 laboratory, École de technologie supérieure (ÉTS), Montreal, Canada. Cation concentrations were determined using an inductively coupled plasma optical emission spectrometer (5110 ICP-OES, Agilent), and anion concentrations were measured with an ion chromatograph (Dionex ED50, Thermo Fisher Scientific). Bicarbonate (HCO_3^{-}) concentrations were calculated from the charge balance equation, and total dissolved solids (TDS) were derived from the sum of ion concentrations.

Stable isotopic composition of the water molecule ($\delta^{18}O$ and $\delta^{2}H$) was measured using a cavity ringdown spectrometer (Picarro L2130-i) at the LG2 laboratory (ÉTS), Montreal, Canada, expressed in ‰ relative to Vienna Standard Mean Ocean Water (VSMOW). Internal reference waters were used for normalization after every 3 injections. The analytical uncertainty is ± 0.13 ‰ for $\delta^{18}O$ and ± 1.5 ‰ for $\delta^{2}H$. The nearest local meteoric water line (LMWL) is established for the Whitehorse area 220 km east of Shár Shaw Tagà (Birks et al., 2004). The LMWL is similar to isotopic compositions found in the Lhù'àän Mân' (Kluane Lake), 25 km east of Shár Shaw Tagà (Brahney et al., 2010). The LMWL is displayed alongside the analyses results as reference (Fig. 6d, Fig. 7d and Fig. 8d).

Radon (^{222}Rn) serves as a natural tracer to detect groundwater exfiltration in streams (Cartwright and Hofmann, 2016). In situ radon activities were measured at four locations in the N1 subsection, including S-RG8 and S-RG9A springs, and at the upstream and downstream ends of the N1 subsection (S-RUP and S-R1, respectively). A portable RAD7 Radon Monitor (Durridge) was used, coupled with the Rad Aqua accessory (Durridge) for radon degassing. Results are reported in Bq m^{-3}, with an analytical uncertainty of ± 220 Bq m^{-3}.

3.3.2 Principal Component Analysis and clustering

Principal Component Analysis (PCA) was employed to classify the origins of the sampled water and to identify sample groups that influence the chemistry of the Shár Shaw Tagà River. For each of the three sampling campaigns, PCA was performed

https://doi.org/10.5194/egusphere-2025-117
Preprint. Discussion started: 20 February 2025

using a set of independent variables: water temperature, $\delta^{18}O$, Na^+, Mg^{2+}, Ca^{2+}, and SO_4^{2-}. These major ions were selected as they exhibited concentrations above the detection limit in more than 95 % of the samples. Principal components explaining at least 90 % of the total variance were retained for further analysis to ensure the robustness of the PCA.

After conducting PCA, clustering analysis was performed using the k-means algorithm for each campaign (Lloyd, 1982; MacQueen, 1967). This analysis was based on the sample scores derived from the selected principal components. The maximum number of clusters was set at 25 % of the total number of samples for each campaign, which corresponded to 5, 9 and 7 for the campaigns of June 2022, August 2022, and June 2023, respectively. The algorithm determined the resulting clusters were by associating samples with dominant combinations of variables, thereby highlighting inherent patterns within the dataset.

3.4 TIR survey

Aerial or handheld thermal infrared (TIR) devices have been demonstrated as effective tools for mapping groundwater discharge into streams (Toran, 2019). Specifically, drone-based TIR technology allows for high spatial resolution observations of surface water-groundwater interactions (Vélez-Nicolás et al., 2021). Two common approaches for TIR surveys were considered: 1) generating stream temperature maps using high-definition TIR image ortho-mosaics from overlapping images (e.g., Abolt et al., 2018; Casas-Mulet et al., 2020; Rautio et al., 2015), and 2) using TIR videos or real-time scans (handheld or drone-based) to visualize mixing plumes and record GPS coordinates of observed points (e.g., Barclay et al., 2022; Briggs et al., 2016; Iwasaki et al., 2023). While georeferenced thermal maps provide mesoscale coverage, they require stable flying conditions, ground control points, and extensive postprocessing (Webb et al., 2008). In contrast, TIR video or live scans allow for real-time visualization of mixing dynamics in smaller-scale areas (Antonelli et al., 2017). Given our goal to identify and characterize groundwater exfiltration zones, we chose the TIR video approach.

Drone-based TIR video surveys were conducted on 28 June 2024, between 8:00 and 10:00, to maximize the coverage of shaded sections of the stream. The surveys were conducted using a DJI Mavic Enterprise 3T, equipped with a DJI RTK module and a DJI D-RTK 2 mobile station for GNSS base-station support. The Mavic 3T features a 48-megapixel RGB camera with a 24 mm focal length and a 640x512-pixel thermal camera with a 40 mm focal length. The drone was manually controlled to optimize the capture of surface temperatures across wide sections of the Shár Shaw Tagà River, recording both TIR and RGB videos simultaneously. Flight altitudes ranged from 5 to 20 m, depending on the section.

The survey began 180 m upstream of the N1 subsection and ended 800 m downstream of the N2 subsection (Fig. 2). Due to difficulties in flying over the “narrow section”, it was surveyed twice at different elevations.

The TIR video was visually analyzed to identify cold groundwater exfiltration areas using two criteria: 1) a clear contrast between the dominant stream surface temperature and the suspected exfiltration area, with an area larger than 10 cm^2, and 2) the presence of a turbulent mixing zone at least 1 meter in length immediately downstream of the suspected area (flight data and information are available as Supplemental Material in Charonnat and Baraer, 2025). When both criteria were met, the

https://doi.org/10.5194/egusphere-2025-117
Preprint. Discussion started: 20 February 2025

RGB video was used for confirmation. The Shár Shaw Tagà River, originating from glacial melt, has a substantial suspended sediment load, whereas groundwater is nearly free of suspended sediments. This contrast is visible in the RGB video frames. Finally, images of confirmed groundwater exfiltration areas were extracted from the videos for size evaluation. Exfiltration areas from the left bank were labeled TIR-L#, and those from the right bank were labeled TIR-R#.

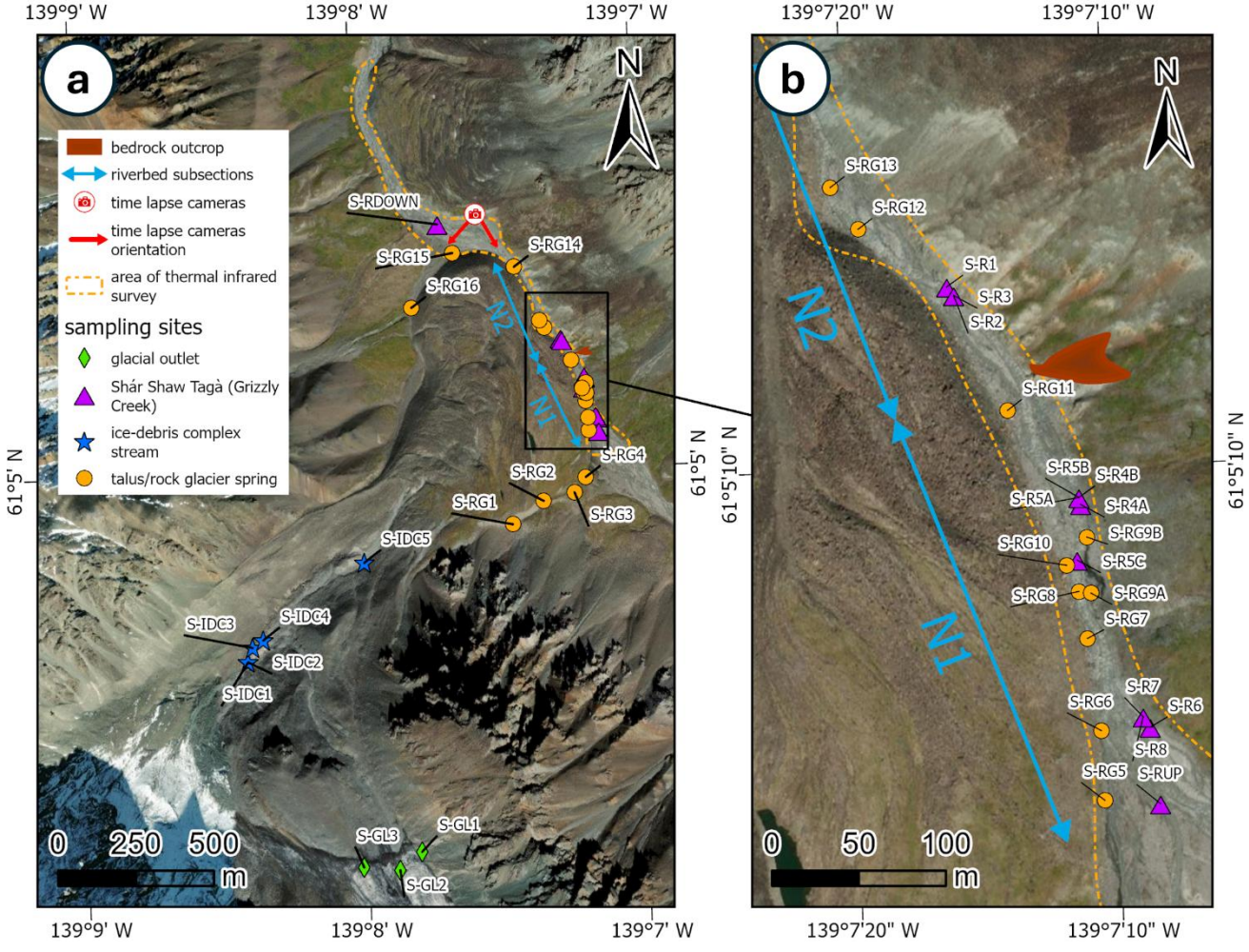

Fig. 2: Map illustrating the methods used in this study. Panel (a) corresponds to the area shown in Fig. 1b, while panel (b) provides a zoom-in of panel (a). A bedrock outcrop on the talus slope opposite to RG-A1 marks the division of the Shár Shaw Tagà River's "narrow section" into two subsections, N1 and N2, as shown on the map. The positions of time-lapse cameras TLC1 and TLC2 are indicated on the southern front of RG-B2, with their southwest and southeast orientations, respectively. The area covered by the drone-based TIR survey extends along the Shár Shaw Tagà riverbed from the northern front of RG-B2 downstream to the southern front of RG-A1, passing through two outwash plains. Sampling sites are depicted with different symbols depending on their type: glacial outlet from the G-B1 snout (S-GL#), Shár Shaw Tagà River (S-R#), ice-debris complex stream (S-IDC#), and springs at RG-A1 front and opposite talus (S-RG#). The spring locations represent the outflow points observed during the August 2022 campaign, though their positions may vary depending on hydro-meteorological conditions. Basemap credits: Esri.

https://doi.org/10.5194/egusphere-2025-117
Preprint. Discussion started: 20 February 2025

4. Results

4.1 TL monitoring

Between 2018 and 2021, TL1 monitored aufeis formation during the winters of 2018-2019 and 2019-2020 (Fig. 3 and 4a). No aufeis formation was observed during the winter of 2020-2021. The onset of aufeis development varied between the two winters: in 2018-2019, it began in early November and continued to develop throughout the winter season, whereas in 2019-2020, it started in February and progressed through February and March (Fig. 3). The development of the aufeis in both winters occurred in phases characterized by multiple flood events. Visible ablation of the aufeis began in May, with complete melt occurring by June in both 2019 and 2020. The aufeis that formed during the winters of 2018-2019 and 2019-2020 spanned the entire width of the river, from the RG-A1 front to the RG-B2 front.

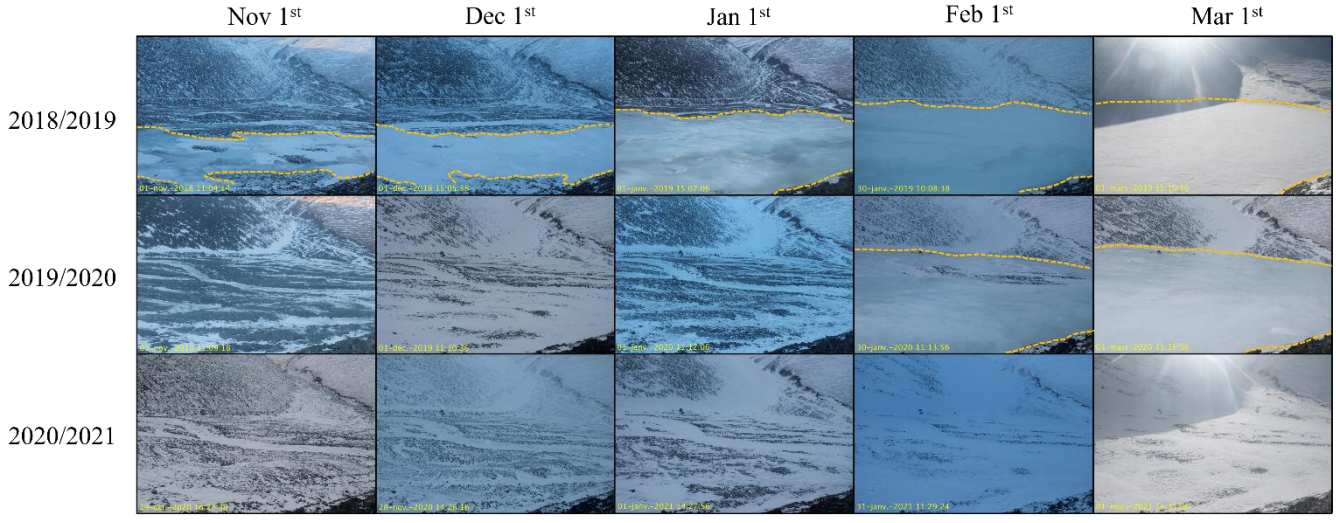

Fig. 3: Monthly timelapse images captured by TL1 of the aufeis from November 1st to March 1st during the winters of 2018-2019, 2019-2020, and 2020-2021. The yellow dashed line indicates the extent of the aufeis in each image when visible. The timelapse images were selected based on the closest date to the first day of each month, with consideration given to image quality. Note that no aufeis formation occurred during the 2020-2021 winter.

TL2, installed in 2019 next to TL1 and oriented upstream, recorded the formation of the aufeis in the winter of 2019-2020 and its absence during 2020-2021. In the winter of 2020, TL2 captured reflections of liquid water and/or ice at the end of the N2 subsection, when the river was dry (Fig. 4). In subsequent days, the aufeis was observed to form in the downstream outwash plain, starting from the end of the N2 subsection. This observation suggests that the overflowing water contributing to the formation of the aufeis originates from the “narrow section” of the Shár Shaw Tagà River.

https://doi.org/10.5194/egusphere-2025-117
Preprint. Discussion started: 20 February 2025

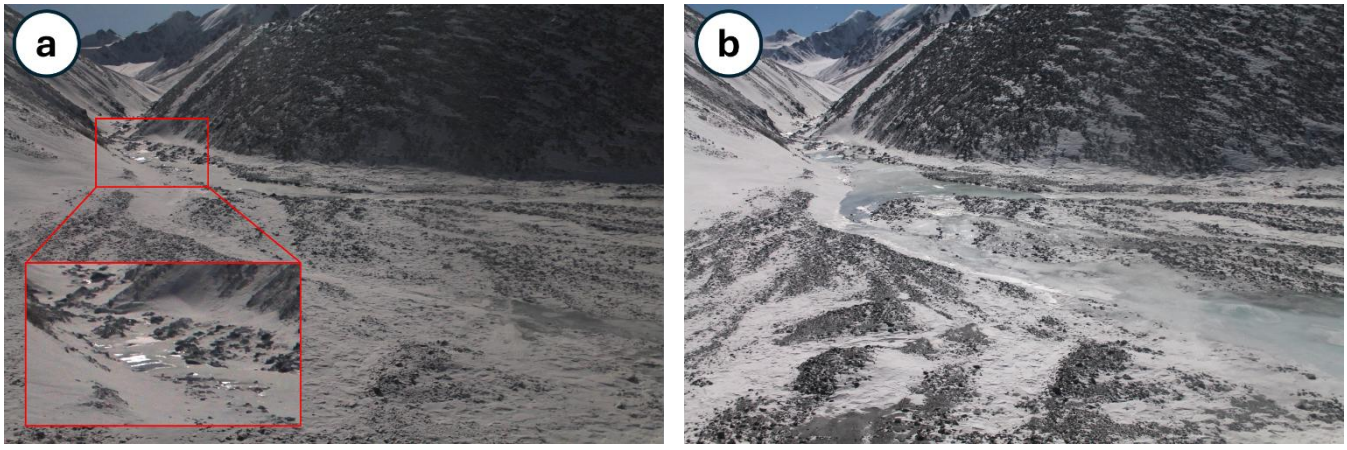

Fig. 4: Initiation of an aufeis in the downstream outwash plain, captured by TL2 on (a) 04/01/2020 at 08:00, and (b) 08/01/2020 at 11:00. The light in the raw images has been enhanced to improve picture quality. Both images are oriented towards the end of the N2 subsection and the entrance of the downstream outwash plain. (a) At 8:00 on 04/01/2020, the aufeis has not yet formed, but reflections of ice and/or liquid water are visible at the end of the N2 subsection, during a time when the Shár Shaw Tagà River is dry. (b) At 11:00 on 08/01/2020, the aufeis has started to form in the outwash plain, extending from the end of the N2 subsection.

The repetitive monitoring of the aufeis provides evidence of overflow events during late fall and winter, particularly in the 2018-2019 and 2019-2020 periods. The formation of the aufeis is attributed to groundwater outflow from the "narrow section" of the Shár Shaw Tagà River, as the river runs dry in winter in the downstream outwash plain and no aufeis forms in the upstream outwash plain. This finding aligns with the high density of springs inventoried along the N1 subsection.

4.2 Physico-hydrochemical characterization

4.2.1 Sampling and field measurements

A high concentration of springs was reported along the N1 subsection of the Shár Shaw Tagà River (S-RG5 to S-RG11) from 2018 to 2021, and during the 2022 sampling campaigns. This led to a dedicated sampling campaign in June 2023. Many of these springs were sampled across multiple campaigns, indicating their long-term flow. The June 2022 and August 2022 sampling campaigns can be directly compared for the springs at RG-A1's front, given their similar spatial coverage and sampling sites. In contrast, the June 2023 sampling campaign focused specifically on the N1 subsection of the river (Table S1).

The mean water temperature for samples collected from the springs at RG-A1's front in June 2022 was 0.90 °C, with a range of 3.16 °C, slightly colder than in samples from August 2022, exhibiting a mean temperature of 1.38 °C and a range of 3.77 °C (Table S2). While cold temperatures in June 2022 may have been strongly influenced by recent snowmelt, no snow remained at the lower elevations of the catchment in August 2022. In late season, cold groundwater outflows (< 2 °C) suggest

https://doi.org/10.5194/egusphere-2025-117
Preprint. Discussion started: 20 February 2025

the possible presence of frozen content in the vicinity of springs (Carturan et al., 2016; Frauenfelder et al., 1998; Haeberli, 1975; Scapozza, 2009).

The June 2022 campaign recorded a lower mean EC in springs at RG-A1's front of 225.64 µS cm^{-1}, with a range of 439.10 µS cm^{-1}, compared to 490.82 µS cm^{-1} with a range of 546.72 µS cm^{-1} in August 2022. These results indicate dilution due to snowmelt in early season and increased groundwater contribution in late season, consistent with results from other rock glacier hydrology studies (Jones et al., 2019). The high EC ranges highlight the heterogeneous behavior of the sampled springs. Mean pH values were 8.47 in June 2022 and 8.13 in August 2022, with ranges of 1.84 and 1.00, respectively.

The mean isotopic composition was more depleted in the springs at RG-A1's front in June 2022 (-23.57 ‰ vs. VSMOW for $\delta^{18}O$ and -183.69 ‰ vs. VSMOW for $\delta^{2}H$, with ranges of 1.64 ‰ and 8.78 ‰, respectively) compared to August 2022 (-21.01 ‰ vs. VSMOW for $\delta^{18}O$ and -169.20 ‰ vs. VSMOW for $\delta^{2}H$, with ranges of 1.38 ‰ and 9.68 ‰, respectively). This depletion is associated with a higher snowmelt contribution in June 2022. Solute concentrations were generally lower in June 2022, frequently falling below detection limits for chlorides (all samples < 0.13 mg L^{-1}), potassium (13 out of 20 samples < 0.01 mg L^{-1}), sodium (13 out of 20 samples < 0.09 mg L^{-1}), and magnesium (1 out of 20 samples < 0.03 mg L^{-1}). In contrast, in August 2022, solute concentrations exceeded detection limits for 38 out of 39 samples for all elements except chlorides (36 out of 39 samples < 0.13 mg L^{-1}).

The June 2023 campaign showed a mean water temperature for the rock glacier springs of 1.40°C, with a range of 0.23 °C. The mean EC value for June 2023 was 678.43 µS cm^{-1}, with a range of 172.00 µS cm^{-1}. The mean pH value was 7.82 with a range of 0.23. The mean isotopic composition for the springs during this campaign was -22.86 ‰ vs. VSMOW for $\delta^{18}O$ and -178.11 ‰ vs. VSMOW for $\delta^{2}H$, with ranges of 0.30 ‰ and 1.10 ‰, respectively.

In June 2023, while the Shár Shaw Tagà River level was lower than in previous years for the same period, ^{222}Rn activities were similar at S-RG8 and S-RG9A, ranging from $10.17\times10^{3} \pm 0.22\times10^{3}$ Bq m^{-3} to $10.85\times10^{3} \pm 0.19\times10^{3}$ Bq m^{-3} (Fig. 5). These springs are located along the N1 subsection of the river, at the left and the right of the stream, respectively. In contrast, the Shár Shaw Tagà River at the upstream end of the N1 subsection (S-RUP) exhibited low activities ($0.36\times10^{3} \pm 0.06\times10^{3}$ Bq m^{-3}), while the downstream end of N1 (S-R1) showed significantly higher activities ($5.46\times10^{3} \pm 0.14\times10^{3}$ Bq m^{-3}). These results indicate a major groundwater input to the Shár Shaw Tagà River in the N1 subsection, where S-RG8 and S-RG9A are located.

https://doi.org/10.5194/egusphere-2025-117
Preprint. Discussion started: 20 February 2025

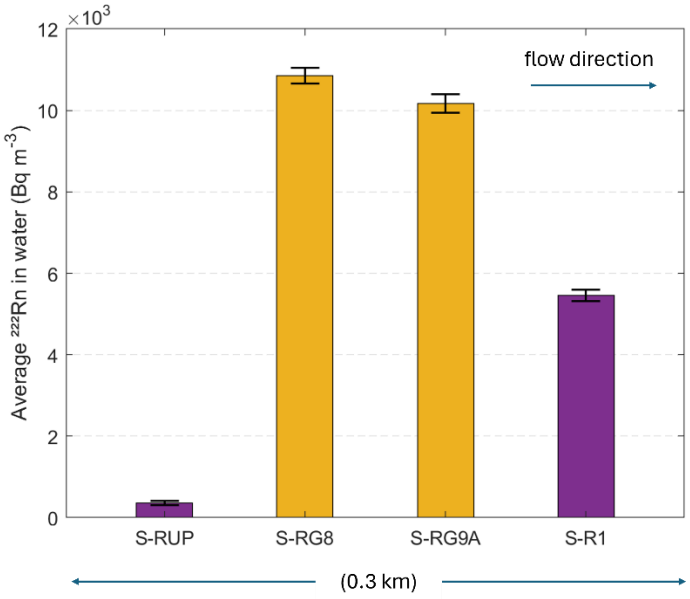

328

329 **Fig. 5: ^{222}Rn activities measured with a portable RAD7 Radon Monitor (Durridge) in June 2023. Data were collected at springs S-**
330 **RG8 and S-RG9A (orange) and along the Shár Shaw Tagà river at upstream (S-RUP) and downstream (S-R1) sites (purple). The**
331 **bars are arranged from left to right in spatial sequence from upstream to downstream. The error bars represent the uncertainties**
332 **in the radon activity measurements.**

333

334 **4.2.2 Principal Component Analysis and clustering**

335 **Samples collected in June 2022**

336 Principal Component (PC) 1 accounts for 60.96 % of the variance in the dataset and primarily reflects the influence of mineral
337 elements, with PC scores ranging from 0.47 to 0.50 (Fig. 6a). PC2 and PC3, explaining 18.29 % and 14.10 % of the variance,
338 respectively, exhibit contrasting associations with the $\delta^{18}O$ ratio and temperature. PC2 displays a strong positive correlation
339 with the $\delta^{18}O$ ratio (0.73) and a negative correlation with temperature (-0.67), whereas PC3 shows positive correlations with
340 $\delta^{18}O$ (0.62) and temperature (0.71).
341 Clustering analysis based on PCA reveals two distinct clusters among the June 2022 samples (Fig. 6b). Cluster 1 comprises
342 17 samples characterized by low concentrations of mineral elements (Fig. 6c), with total dissolved solids (TDS) concentrations
343 ranging from 28 to 100 mg L^{-1}. In contrast, Cluster 2 includes samples S-RG4, S-RG5, and S-RG8, which show elevated TDS
344 values (90 to 269 mg L^{-1}). With the exception of S-RUP, S-RG4, and S-RG15, which record warmer temperatures from 1.43
345 to 3.19 °C, the remaining 16 samples in the June 2022 dataset exhibit colder temperatures, ranging from 0.03 °C to 0.67 °C
346 (Fig. 6c). The most enriched samples are S-RG7, S-RG8, and S-RG10, with $\delta^{18}O$ values between -23 ‰ and -22.6 ‰ vs.
347 VSMOW in $\delta^{18}O$.

https://doi.org/10.5194/egusphere-2025-117
Preprint. Discussion started: 20 February 2025

In June 2022, most of the springs were supplied by recent snowmelt, as indicated by low concentrations of mineral elements and cold temperatures. In contrast, S-RG8 and S-RG4 were supplied by groundwater, as evidenced by their higher concentrations of mineral elements.

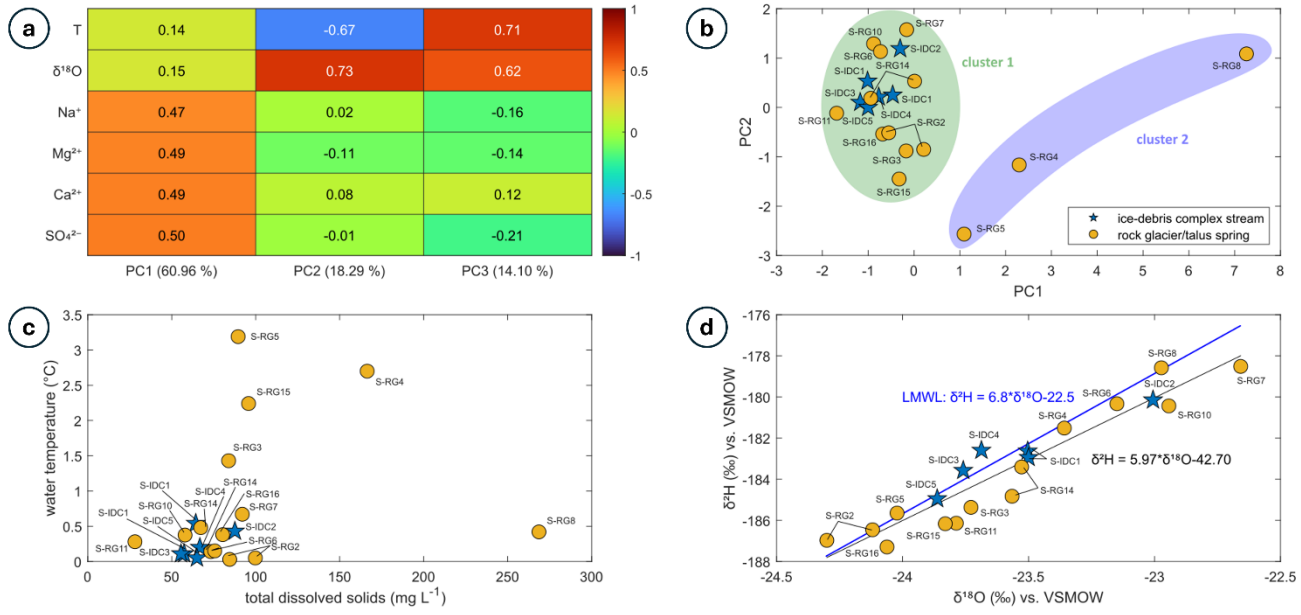

Fig. 6: (a) PCA scores for June 2022 samples. Scores are displayed for PC1, PC2, and PC3, which together account for over 90% of explained variance. The six variables used in the analysis are water temperature (T), $\delta^{18}O$, Na^+, Mg^{2+}, Ca^{2+}, and SO_4^{2-} concentrations. The explained variance for each PC is indicated in the legend of the horizontal axis. (b) Distribution of clusters formed from June 2022 samples following PCA and k-means clustering. Symbols represent different sample types, and ellipses illustrate the distribution of each cluster. (c) Distribution of total dissolved solids (TDS) concentrations and water temperature for the June 2022 samples. Symbols represent different sample types. (d) Isotopic composition of the June 2022 samples. Symbols represent sample types. The black line represents the linear regression for the June 2022 samples, defined as $\delta^2H = 5.97*\delta^{18}O-42.70$. The blue line represents the nearest local meteoric water line (LMWL), established for the Whitehorse area, located 220 km east of the Shár Shaw Tagà catchment (Birks et al., 2004). This line is similar to the isotopic compositions found in the Lhù'ààn Mân' (Kluane Lake), 25 km east (Brahney et al., 2010).

Samples collected in August 2022

PC1 accounts for 60.57 % of the variance in the dataset and is strongly influenced by solute concentrations, with PC scores ranging from 0.47 to 0.48 (Fig. 7a). PC2, which explains 22.34 % of the variance, reflects opposing influences of temperature (0.68) and isotopic composition (-0.63). PC3, accounting for 9.01 % of the variance, shows joint positive correlations with both temperature (0.71) and isotopic composition (0.63).

Clustering analysis clearly distinguishes different sample types, forming 9 clusters, the maximum achievable based on the parametrization (Fig. 7b). Cluster 3 consists of glacial outlet samples, characterized by low solute concentrations (16 to 38 mg L^{-1} in TDS), cold temperatures (0.06 to 0.07 °C), and depleted isotopic compositions (-21.6 to -22 ‰ vs. VSMOW in $\delta^{18}O$) as

https://doi.org/10.5194/egusphere-2025-117
Preprint. Discussion started: 20 February 2025

seen in Figs. 7c and 7d. Clusters 5 and 6 comprise Shár Shaw Tagà River samples, with warmer temperatures (3.47 °C to 6.26 °C), higher solute concentrations (88 to 238 mg L^{-1} in TDS), and depleted isotopic compositions (-21.8 to -22.2 ‰ vs. VSMOW in $\delta^{18}O$). The distinction between these clusters may be attributed to variations in the glacial regime diurnal cycle and weather conditions based on sampling times. Clusters 4 and 8 include samples from springs near the upper end of the rock glacier front and at the transition area with the ice-debris complex (e.g., S-IDC5, S-RG1, S-RG2). As shown in Figs. 7c and 7d, these springs display high concentrations of mineral elements (209 to 304 mg L^{-1} in TDS) and enriched isotopic compositions (-20.6 to -20.9 ‰ vs. VSMOW in $\delta^{18}O$). Clusters 2 and 9 are represented by springs S-RG7, S-RG8, S-RG9A, and S-IDC1, which exhibit high but narrow ranges of solute concentrations (282 to 309 mg L^{-1} in TDS) and more depleted isotopic compositions (-21.6 to -21.8 ‰ vs. VSMOW in $\delta^{18}O$), as shown in Fig. 7d. Clusters 1 and 7 include other springs from the N1 subsection of the Shár Shaw Tagà River, which are characterized by low solute concentrations (111 to 162 mg L^{-1} in TDS) and enriched isotopic compositions (-20.4 to -20.9 ‰ vs. VSMOW in $\delta^{18}O$). Fig. 7d clearly distinguishes samples with depleted isotopic compositions (below -21.5 ‰ vs. VSMOW in $\delta^{18}O$) from those with enriched compositions (above -20.9 ‰ vs. VSMOW in $\delta^{18}O$).

In late summer, the hydrochemical signatures of the springs show significant contrasts, with a high number of clusters. However, springs S-RG7, S-RG8, and S-RG9A share isotopic signatures similar to glacial meltwater from S-G1, S-G2, and S-G3, indicating a glacial input. Despite being located on opposite sides of the river, these springs cluster together, contrasting with the other springs. The high number of clusters among the other springs, with more enriched isotopic compositions, is likely due to different local drainage systems influenced by summer precipitation. Interactions between the groundwater sources of these two spring types may explain the varying clustering patterns and physicochemical values observed for RG-7 and RG-8. Most of the rock glacier spring samples show very cold temperatures (< 2 °C; Fig. 7c), suggesting proximity to massive ice or permafrost areas (e.g. Carturan et al., 2016).

https://doi.org/10.5194/egusphere-2025-117
Preprint. Discussion started: 20 February 2025

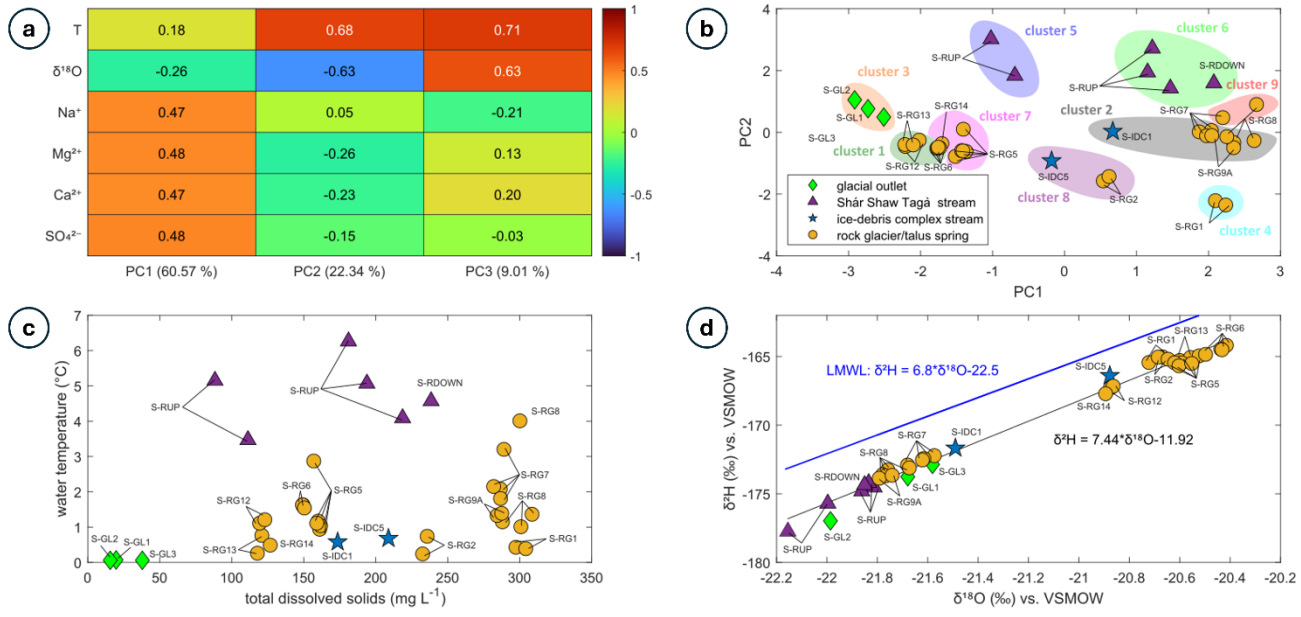

Fig. 7: (a) PCA scores for August 2022 samples. Scores are displayed for PC1, PC2, and PC3, which together account for over 90% of explained variance. The six variables used in the analysis are water temperature (T), $\delta^{18}O$, Na^+, Mg^{2+}, Ca^{2+}, and SO_4^{2-} concentrations. The explained variance for each PC is indicated in the legend of the horizontal axis. (b) Distribution of clusters formed from August 2022 samples following PCA and k-means clustering. Symbols represent different sample types, and ellipses illustrate the distribution of each cluster. (c) Distribution of total dissolved solids (TDS) concentrations and water temperature for the August 2022 samples. Symbols represent different sample types. (d) Isotopic composition of the August 2022 samples. Symbols represent sample types. The black line represents the linear regression for the August 2022 samples, defined as $\delta^2H = 7.44*\delta^{18}O-11.92$. The blue line represents the nearest local meteoric water line (LMWL), established for the Whitehorse area, located 220 km east of the Shár Shaw Tagà catchment (Birks et al., 2004). This line is similar to the isotopic compositions found in the Lhù'ààn Mân' (Kluane Lake), 25 km east (Brahney et al., 2010).

Samples collected in June 2023

PCA conducted on samples collected in June 2023 revealed that PC1 accounts for 68.79 % of the variance (Fig. 8a), primarily driven by solute concentrations (PC scores ranging from 0.40 to 0.48). PC2 and PC3 explain 15.54 % and 10.43 % of the variance, respectively. PC2 is mainly influenced by water temperature (0.88), while PC3 is dominated by isotopic composition (0.86).

The glacier outlet samples form a distinct cluster, labeled as Cluster 3 (Fig. 8b). The remaining samples are divided into two clusters, with a clear distinction based on the maximum number of clusters (5). Cluster 1 consists solely of Shár Shaw Tagà River samples from the upstream part of the N1 subsection. Cluster 2 includes spring samples and Shár Shaw Tagà River samples collected in the downstream part of the N1 subsection. River samples from the downstream N1 subsection and spring samples exhibit higher solute concentrations (from 121 to 147 mg L^{-1} in TDS) and colder temperatures (from 0.7 to 4 °C, with 14 out of 16 samples < 2 °C) compared to the upstream N1 samples, which have lower solute concentrations (87 to 125 mg L^{-}

https://doi.org/10.5194/egusphere-2025-117
Preprint. Discussion started: 20 February 2025

[1]) and warmer temperatures (5.3 to 9.5 °C; Fig. 8c). The isotopic composition is generally more enriched for the upstream N1 river samples than for the downstream N1 river and spring samples (Fig. 8d). The isotopic composition of one of the two glacial water samples from G-B1 (sample S-GL1) is similar to the composition from the Shár Shaw Tagà River in upstream N1 (water flowing from G-A1). However, the second S-GL1 sample shows a much more enriched isotopic composition, due to a two-day interval between the respective samplings. The most enriched sample (-21.2 ‰ vs. VSMOW in $\delta^{18}O$ and -165.4 ‰ vs. VSMOW in $\delta^{2}H$) was taken first, when the G-B1 glacier was still snow-covered. The most depleted sample (-22.4 ‰ vs. VSMOW in $\delta^{18}O$ and -173.6 ‰ vs. VSMOW in $\delta^{2}H$) was taken two days later, following significant snowmelt cover on G-B1 and the initiation of glacial melt.

The springs located on opposite sides of the river along the N1 subsection cluster together and exhibit similar hydrochemical signatures, similar to what was observed in August 2022. By distinguishing between two clusters, the PCA highlights the important influence of these springs on the Shár Shaw Tagà River. Their outflows significantly lower the water temperature and increase solute concentrations in the river.

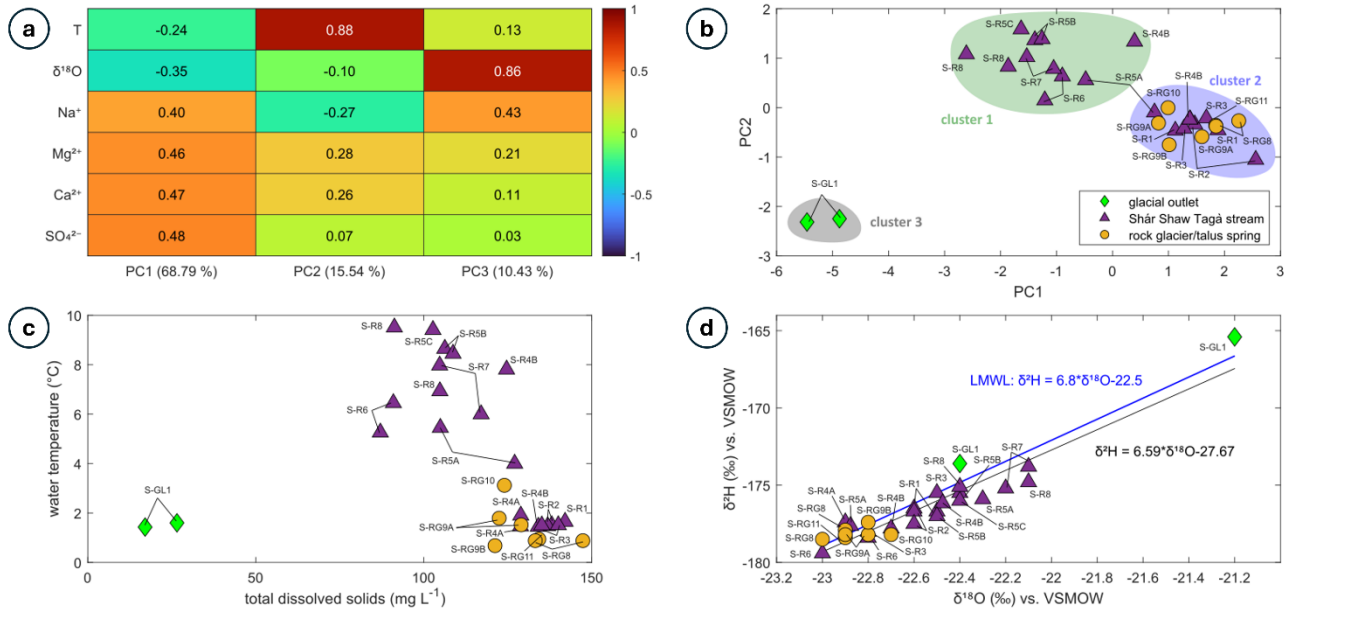

Fig. 8: (a) PCA scores for June 2023 samples. Scores are displayed for PC1, PC2, and PC3, which together account for over 90% of explained variance. The six variables used in the analysis are water temperature (T), $\delta^{18}O$, Na^{+}, Mg^{2+}, Ca^{2+}, and SO_4^{2-} concentrations. The explained variance for each PC is indicated in the legend of the horizontal axis. (b) Distribution of clusters formed from June 2023 following PCA and k-means clustering. Symbols represent different sample types, and ellipses illustrate the distribution of each cluster. (c) Distribution of total dissolved solids (TDS) concentrations and water temperature for the June 2023 samples. Symbols represent different sample types. (d) Isotopic composition of the June 2023 samples. Symbols represent sample types. The black line represents the linear regression for the June 2023 samples, defined as $\delta^{2}H = 6.59*\delta^{18}O-27.67$. The blue line represents the nearest local meteoric water line (LMWL), established for the Whitehorse area, located 220 km east of the Shár Shaw Tagà catchment (Birks et al., 2004). This line is similar to the isotopic compositions found in the Lhù'ààn Mân' (Kluane Lake), 25 km east (Brahney et al., 2010).

https://doi.org/10.5194/egusphere-2025-117
Preprint. Discussion started: 20 February 2025

Synthesis of physico-hydrochemical characterisation

The springs surrounding RG-A1's front exhibit heterogeneous hydrochemical signatures. However, a group of springs along the N1 subsection (S-RG7, S-RG8, and S-RG9A) cluster together in PCA and share high EC values, depleted isotopic compositions, high solute concentrations, and similar radon activities. Despite being located on opposite sides of the river, these three springs show striking similarities, suggesting a common origin. Their isotopic compositions are comparable to those of glacial meltwater sampled at G-B1 and in the Shár Shaw Tagà River, differing significantly from other springs along RG-A1's front. The contribution of internal ice melt in rock glacier outflows is known to be minimal and does not significantly influence isotopic signatures (Croce and Milana, 2002; Krainer and Mostler, 2002; Krainer et al., 2007). This evidence supports the conclusion that S-RG7, S-RG8, and S-RG9A are springs fed by shallow groundwater of glacial origin.

During low-discharge periods, such as June 2023, the springs along the N1 subsection considerably increase downstream solute concentrations and radon activities in the Shár Shaw Tagà River, while their cold outflows reduce stream temperature. The other springs around RG-A1's front are primarily supplied by snowmelt in early summer and by summer precipitation in late summer. Their diverse hydrochemical signatures and resulting clusters reflect varying local drainage systems within the rock glacier. Springs at the front of RG-A1 consistently exhibit cold temperatures, indicating their proximity to ground ice.

4.3 TIR survey

The TIR survey detected four cold water outflows outside the "narrow section" of the Shár Shaw Tagà River, located in the outwash plain downstream of RG-A1 (Fig. 9). Two outflows were identified on the left bank: one associated with meltwater originating from a snow patch at the front of RG-A1, and the other is from a persistent snow patch on the west flank of the valley. The other two outflows were located on the right bank, originating from the middle of the outwash plain near the front of RG-B2. These four outflows are not supplied by RG-A1, as they originate from snow patches or from the right bank.

The furthest downstream exfiltration area in the "narrow section" (TIR-L8) is situated in the N1 subsection, just a few meters upstream of the bedrock outcrop (Fig. 9). Within the N1 subsection, eight groundwater exfiltration areas were identified on the left bank of the main channel, and six on the right bank. Exfiltration areas on the left bank are generally smaller, with plume lengths ranging from 1 to 6 m, four of these less than 2 m long. In contrast, exfiltration areas on the right bank are larger, with plume lengths ranging from 5 to 14 m, and four exceed 10 m in length. These exfiltration areas were clearly visible as color contrasts, distinguishing the warmer surface waters from the colder groundwater exfiltrations (Fig. 10a). The positions of the mixing plumes were observed at each location. In the most notable exfiltration areas (plume lengths > 2 m), clearer water was observed in the visible video footage, facilitating the validation of groundwater exfiltration detection (Fig. 10b).

Two of the six groundwater exfiltration areas detected from the right bank can be associated with springs sampled and measured during the 2022 and 2023 campaigns for physico-hydrochemical analysis (TIR-R2 and TIR-R3 correspond to S-RG9A and S-RG9B, respectively). As mentioned in Sect. 2, depending on the river level and meteorological conditions, the outflow locations of the springs on the left side of the river have been observed to shift 10 to 20 m downstream of the RG-A1

https://doi.org/10.5194/egusphere-2025-117
Preprint. Discussion started: 20 February 2025

front. During the TIR survey, these conditions were met, and no exfiltration area was found directly at the location of a spring sampled in 2022 and 2023. Instead, exfiltration areas on the left bank were detected 20 m downstream of their corresponding springs sampled earlier. Therefore, exfiltration areas TIR-L1, TIR-L2 and TIR-L8 can be associated with the springs S-RG8, S-RG10 and S-RG11, respectively (Fig. 9).

The drone-based TIR survey identified a high density of cold groundwater exfiltrations from both the left and right banks of the N1 subsection of the Shár Shaw Tagà River, upstream of the bedrock outcrop. Exfiltration areas on the right bank exhibited longer plumes, suggesting higher discharge. Two cold outflows were detected in the downstream outwash plain on the left bank, but no groundwater origin was identified for these.

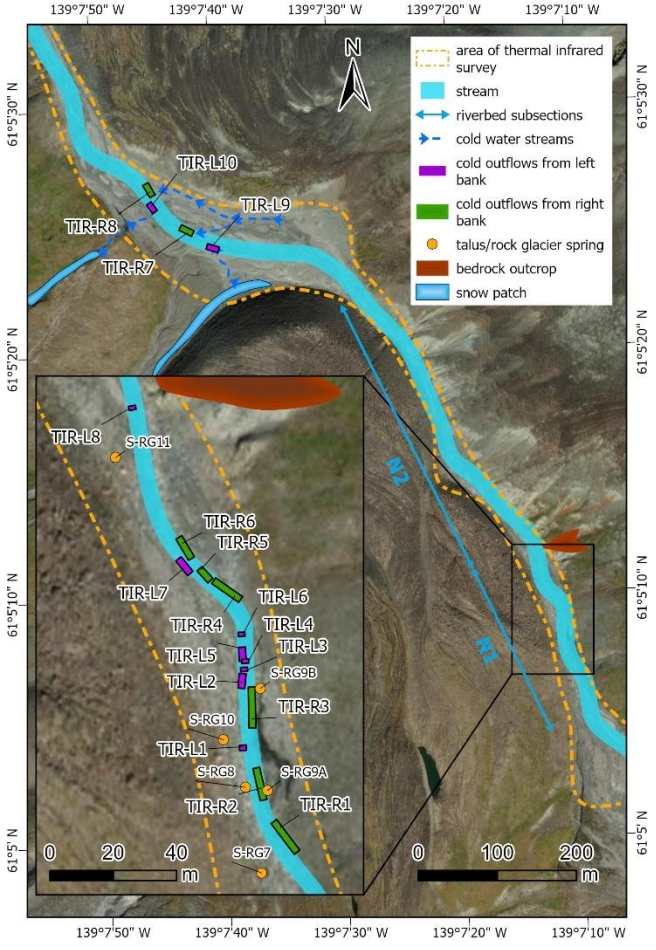

Fig. 9: Location of cold water outflows detected by the TIR survey along the Shár Shaw Tagà riverbed. The zoomed-in view of the "narrow section" highlights an area with a high density of cold groundwater outflows detected on both sides of the river, upstream of a bedrock outcrop constraining the riverbed. Additional cold water outflows are observed in the downstream outwash plain, originated from either snow patch melt on the left side or from the right bank of the outwash plain. Springs that outflow from RG-A1 or the opposite talus slope and were sampled during the 2022 and 2023 campaigns are marked in the zoomed-in panel. The spring locations represent the positions of their outflows during the August 2022 campaign, though these may shift depending on hydro-meteorological conditions and river level. The bedrock outcrop marks the division of the "narrow section" of the Shár Shaw Tagà River into two subsections, N1 and N2, as shown on the map. Basemap credits: Esri.

https://doi.org/10.5194/egusphere-2025-117
Preprint. Discussion started: 20 February 2025

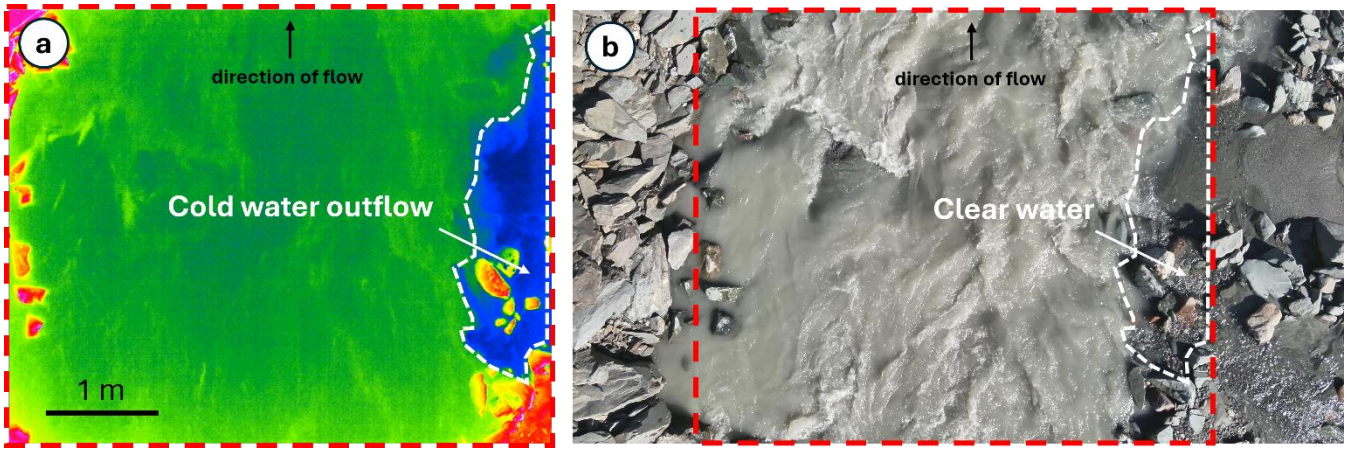

Fig. 10: (a) TIR capture showing cold groundwater outflow (in blue, delimited by the dashed white line), mixing with the warmer waters of the Shár Shaw Tagà River (in green) at the TIR-R2 location. Note that the video does not provide a color scale. (b) RGB image capture showing clear water outflowing into the Shár Shaw Tagà River, which is characterized by a significant sediment load at the TIR-R2 location. The cold water area detected with TIR is delimited by the dashed white line. The extent of the TIR capture is indicated by the dashed red line. Flight data and information can be accessed as Supplemental Material in Charonnat and Baraer, 2025.

5 DISCUSSION

5.1 The rock glacier forces resurgence of shallow groundwater flow

The preliminary inventory of springs and the TIR survey identified a high density of spring outflows from both banks of the N1 subsection of the Shár Shaw Tagà River. The physico-hydrochemical characterization indicates that the springs on both banks share a similar signature, originating from glacial melt, suggesting a common source. In June 2023, a low-discharge period, field observations revealed river water losses before entering the upstream outwash plain, where the riverbed temporarily lacked surface flow. Surface flow resumed only from the N1 subsection due to groundwater inflows, pointing to the existence of shallow subsurface flow through the upstream outwash plain. Together, these elements indicate that water outflowing from the springs along the N1 subsection resurges from lateral shallow groundwater, likely infiltrating through the riverbed and flowing within the lateral alluvial aquifer before resurfacing.

Contrary to initial hypotheses, no evidence was found of outflow supplied by the head of the rock glacier's subcatchment (comprising glaciers G-B1 and G-B2). The physico-hydrochemical characterization instead suggests that glacial meltwater outflowing to the river originates from the upstream outwash plains of the main Shár Shaw Tagà catchment. The characterization of the other springs at the rock glacier's front suggests that they are linked to local drainage systems within the rock glacier. They are supplied by snowmelt in early season and summer precipitation in late season, with minimal or negligible glacier melt contribution, as shown by the physico-hydrochemical characterization of the samples from June 2022

https://doi.org/10.5194/egusphere-2025-117
Preprint. Discussion started: 20 February 2025

and August 2022, respectively. Some springs may be influenced by both systems, with their physicochemical parameters and clustering reflecting these dual influences depending on hydro-meteorological conditions and time periods.

Parafluvial flow is common in outwash plains with coarse-grained unconsolidated sediments, occurring in river reaches where water is lost before rejoining the river in gaining reaches (Cartwright and Hofmann, 2016). Outwash plains, often underlain by bedrock, retaining groundwater in the shallow subsurface, providing baseflow during dry periods when upstream discharge is limited (Müller et al., 2024). Fractured and faulted bedrock aquifers can further contribute to baseflow in outwash plains (Hayashi, 2019; Müller et al., 2022). In this case, the resurgence of parafluvial and shallow groundwater flow is visible during dry periods. The dynamic location of the springs reported between sampling campaigns reflects the lateral and vertical extent of the alluvial aquifer. The lower density of springs identified beyond the bedrock outcrop at the end of the N1 subsection suggests a shallow bedrock interface with limited groundwater flow capacity. Additionally, the faults inferred along the riverbed in previous geological studies (Dodds and Campbell, 1992) may facilitate groundwater flow from outwash plains upstream of the rock glacier to the N1 subsection, where it is forced to resurge.

The cold temperatures measured in the springs of the N1 subsection indicate that outflows from the alluvial aquifer are cooled by adjacent frozen content. Frozen content has been confirmed in the rock glacier by Evin et al. (1997), and is suspected for the talus slope, based on Scapozza, (2015). The frozen content on both sides of the Shár Shaw Tagà River constrains the alluvial aquifer, forcing groundwater to resurface through springs and cold water upwellings in the riverbed. The advance of the rock glacier, which considerably narrows the riverbed, further enforces this constraint. The younger lobes of the rock glacier, potentially containing higher amounts of frozen content, extend north from the bedrock outcrop to the downstream outwash plain, possibly acting as an additional barrier to groundwater flow where they border the Shár Shaw Tagà River. Thus, the location of the resurgences in the N1 subsection can be explained by the geomorphic properties of the rock glacier. The narrowing of the riverbed by the rock glacier's advance and the presence of frozen content constrain the riverbed, forcing the resurgence of shallow groundwater flow.

5.2 The rock glacier affects downstream cryo-hydrological processes and hydrological continuity

The proximity of bedrock and ground ice in the narrow section of the Shár Shaw Tagà River critically reduces the width and depth of the alluvial aquifer, leading to groundwater exfiltrations along the N1 subsection, as discussed in Sect. 5.1. The TL monitoring suggests that the resurgences from the alluvial aquifer, in combination with a decrease in river flow velocity and channel depth in the outwash plain immediately downstream of the rock glacier, contribute to the formation of aufeis. Thus, the rock glacier plays a significant role in influencing downstream cryo-hydrological processes.

The high density of springs along the N1 subsection and their distinct physicochemical signatures substantially affect the downstream Shár Shaw Tagà River. The physico-hydrochemical characterization from June 2023 demonstrates that during dry periods, these springs notably increase solute concentrations and radon activities, while simultaneously cooling the river water. These findings are consistent with prior studies showing the influence of rock glaciers on the physicochemical

https://doi.org/10.5194/egusphere-2025-117
Preprint. Discussion started: 20 February 2025

characteristics of downstream surface waters (e.g., Bearzot et al., 2023; Brighenti et al., 2023; Robinson et al., 2022; Wagner et al., 2021). However, the rock glacier in this study alters the entire riverbed and its physicochemical parameters primarily due to its geomorphic properties. Contrary to initial hypotheses based on early observations and the literature, its internal hydrological behavior does not account for the critical impact the rock glacier has on the riverbed's hydrological system.

5.3 Future evolution of the rock glacier influence on catchment hydrology

Predicting the future evolution of the system described in Sect. 5.1 and 5.2 is challenging. However, several scenarios across different timescales can be envisioned. Frozen content is likely to persist in depositional landforms for extended periods, as residual ice has been detected in rock glaciers below the modeled elevation limit in multiple cases (e.g., Carturan et al., 2024; Colucci et al., 2019). Future hydrological conditions in alpine catchments will likely be characterized by a reduced hydrological influence of glaciers, lower discharge and an increased contribution from groundwater and periglacial features to streamflow (Huss et al., 2017; Jones et al., 2019; Zierl and Bugmann, 2005). These conditions were observed during the June 2023 sampling campaign, which occurred after the peak of snowmelt and prior to the peak of glacial ablation, leading to a substantial influence of groundwater resurgences on the Shár Shaw Tagà River. Similar conditions may be expected in the future, with groundwater outflows caused by the rock glacier expected to gain influence in the Shár Shaw Tagà River. However, the degradation of frozen content around the riverbed may alter this scenario, as rising air temperatures continue to drive permafrost thaw. Additionally, thermal and mechanical erosion caused by lateral groundwater flow could expand the parafluvial zone and create alternative subsurface flow paths, reducing the hydrological discontinuity and disruptive effects of the rock glacier.

The absence of evident streamflow contribution from the G-B1 subcatchment to the Shár Shaw Tagà River, as highlighted in Sect. 5.1, suggests substantial deep infiltration of surface and shallow groundwater flow between the glaciers of the subcatchment and the rock glacier. Although the role of rock glaciers in deep infiltration has not been thoroughly documented to our knowledge, it is suggested that their high vertical and horizontal flow transmissivity may enhance infiltration into deep aquifers and groundwater recharge (Navarro et al., 2023). From a broader perspective, it is considered that deep groundwater systems link mountain cryosphere components to lowlands aquifers through mountain-block recharge (van Tiel et al., 2024). In this context, increased infiltration due to glacial retreat and permafrost degradation may position rock glaciers and other depositional features as critical hubs in proglacial areas, contributing to regional groundwater circulation and water resources.

5.4 Limitations and perspectives

The physico-hydrochemical characterization conducted in this study was based on three sampling campaigns under varying hydro-meteorological conditions. These diverse settings posed several challenges for water sampling, including issues with accessibility, safety concerns, periods of no flow, and the need to prioritize specific areas. As a result, some sampling sites could not be revisited during every campaign, leading to gaps in the data over time. Moreover, fluctuating weather conditions

https://doi.org/10.5194/egusphere-2025-117
Preprint. Discussion started: 20 February 2025

during a single campaign in proglacial environments likely contributed to variations in physicochemical parameters at some sites. Where possible, multiple samples were taken at different times or on different days within the same campaign to minimize biases caused by diurnal and meteorological variations. Consequently, some sites could not be compared across campaigns, and their characterization can remain incomplete. On the other hand, these challenges allowed us to identify the varying influences of different drainage systems on certain springs.

Upon initial observations and hypotheses, we adopted a unique multi-method approach, which evolved as we refined our understanding of the system. While this combination of methods was crucial in addressing the research question and drawing the conclusions presented, alternative approaches could have provided a more direct route to the findings. Future research could build on the insights gained in this study by investigating the hydrological roles of other rock glaciers within the same valley or in different regions. Such studies would help assess whether similar patterns occur across varying settings. Moreover, this research underscores the potential role of the rock glacier and adjacent depositional features in facilitating the infiltration of water into deep groundwater systems, as suggested by the lack of water outflow from the head of the subcatchment to the the Shár Shaw Tagà River. Characterizing these transfers is crucial for understanding the role of proglacial areas in water resource supply during deglaciation. The authors strongly encourage further works in this direction.

6 CONCLUSIONS

The geomorphic properties of rock glaciers make them dynamic features capable of altering riverbed hydrological systems. As assessed in this study, rock glaciers can obstruct proglacial outwash plains, thereby controlling and constraining shallow groundwater flow. This obstruction results in channel confinement, which induces resurgences from the alluvial aquifer, with profound impacts on both the hydrochemistry and hydrogeomorphology of alpine catchments. Rock glacier disruption leads to substantial changes in the physicochemical parameters of streamflow, and contributes to the formation of aufeis, a consequence not previously documented in the literature.

In contrast to initial hypotheses, the internal hydrological system of the rock glacier does not exhibit a significant influence on downstream surface waters. Instead, the critical disruption to the riverbed hydrological system is due to the geomorphic constraint imposed by the rock glacier on the alluvial aquifer. The water that flows from the subcatchment above the rock glacier is suspected to infiltrate deep groundwater systems through the rock glacier and the adjacent depositional features, as it could not be traced beyond the rock glacier.

Thus, this study emphasizes the complexity and potentially misleading nature of characterizing groundwater flow pathways in proglacial environments. The findings also have broader implications for mountain hydrology and water resources, highlighting the importance of rock glaciers and proglacial systems as critical hydrological features and potential hubs for mountain-block recharge, linking the mountain cryosphere to deep groundwater systems.

https://doi.org/10.5194/egusphere-2025-117
Preprint. Discussion started: 20 February 2025

Code/Data availability

The data supporting this study are available upon request to the corresponding author.

Video supplement

The videos and flight data used for the TIR analysis are available as Supplemental Material in Charonnat and Baraer, 2025, on Borealis dataverse (https://doi.org/10.5683/SP3/O57OMY).

Author contribution

Conceptualization: B.C. and M.B. Data curation: B.C. Formal analysis: B.C., M.B., J.M.-D. and C.M. Funding acquisition: M.B. and J.M.M. Investigation: B.C., M.B., E.V., J.M.-D., K.W. and E.D. Methodology: B.C., M.B., E.V. and J.M.-D. Project administration: B.C., M.B., E.V. and J.M.-D. Supervision: M.B., J.M.-D. and J.M.M. Visualization: B.C. and K.W. Writing – original draft preparation: B.C. Writing – review & editing: B.C., M.B., E.V., J.M.-D., C.M., K.W., E.D. and J.M.M. All authors have read and agreed to the published version of the manuscript.

Competing interests

The authors declare that they have no conflict of interest.

Acknowledgements

We are grateful to the Kluane First Nation and the White River First Nation for the opportunity to conduct research on their territory. We thank the Arctic Institute of North America and the University of Calgary for providing us service and access to their facilities at Kluane Lake Research Station. We thank Parks Canada for their collaboration and for issuing permits that allowed us to conduct research within Kluane National Park and Reserve.

Financial support

This research was supported by the Natural Sciences and Engineering Research Council of Canada, grant numbers RGPIN-2020-05612 and RGPNS-2020-05612, and by Natural Resources Canada—Polar Continental Shelf Program, grant number 62723. Additional funding for the expedition was provided by the Research Centre on the Dynamics of the Earth System (GEOTOP).

https://doi.org/10.5194/egusphere-2025-117
Preprint. Discussion started: 20 February 2025

References

Abolt, C., Caldwell, T., Wolaver, B., and Pai, H.: Unmanned aerial vehicle-based monitoring of groundwater inputs to surface waters using an economical thermal infrared camera, Optical Engineering, 57(05), 1, https://doi.org/10.1117/1.oe.57.5.053113, 2018.

Antonelli, M., Klaus, J., Smettem, K., Teuling, A. J., and Pfister, L.: Exploring Streamwater Mixing Dynamics via Handheld Thermal Infrared Imagery, Water, 9(5), Article 5, https://doi.org/10.3390/w9050358, 2017.

Arenson, L. U., Harrington, J. S., Koenig, C. E. M., and Wainstein, P. A.: Mountain Permafrost Hydrology—A Practical Review Following Studies from the Andes, Geosciences, 12(2), Article 2, https://doi.org/10.3390/geosciences12020048, 2022.

Baker, E. A., Lautz, L. K., Kelleher, C. A., and McKenzie, J. M.: The importance of incorporating diurnally fluctuating stream discharge in stream temperature energy balance models, Hydrological Processes, 32(18), 2901–2914, https://doi.org/10.1002/hyp.13226, 2018.

Baraer, M., McKenzie, J., Bury, J., and Knox, S.: Characterizing contributions of glacier melt and groundwater during the dry season in a poorly gauged catchment of the Cordillera Blanca (Peru), Advances in Geosciences, 22, 41–49, https://doi.org/10.5194/adgeo-22-41-2009, 2009.

Baraer, M., McKenzie, J., Mark, B. G., Gordon, R., Bury, J., Condom, T., Gomez, J., Knox, S., and Fortner, S. K.: Contribution of groundwater to the outflow from ungauged glacierized catchments: A multi-site study in the tropical Cordillera Blanca, Peru, Hydrological Processes, 29(11), Article 11, https://doi.org/10.1002/hyp.10386, 2015.

Barclay, J. R., Briggs, M. A., Moore, E. M., Starn, J. J., Hanson, A. E. H., and Helton, A. M.: Where groundwater seeps: Evaluating modeled groundwater discharge patterns with thermal infrared surveys at the river-network scale, Advances in Water Resources, 160, 104108, https://doi.org/10.1016/j.advwatres.2021.104108, 2022.

Barsch, D.: Rockglaciers: Indicators for the present and former geoecology in high mountain environments, 1996.

Bearzot, F., Colombo, N., Cremonese, E., di Cella, U. M., Drigo, E., Caschetto, M., Basiricò, S., Crosta, G. B., Frattini, P., Freppaz, M., Pogliotti, P., Salerno, F., Brunier, A., and Rossini, M.: Hydrological, thermal and chemical influence of an intact rock glacier discharge on mountain stream water, Science of The Total Environment, 876, 162777, https://doi.org/10.1016/j.scitotenv.2023.162777, 2023.

Birks, S. J., Edwards, T. W. D., Gibson, J. J., Drimmie, R. J. and Michel, F. A.: Canadian network for isotopes in Precipitation, http://www.science.uwaterloo.ca/~twdedwar/cnip/cniphome.html, 2004.

Blöthe, J. H., Rosenwinkel, S., Höser, T., and Korup, O.: Rock-glacier dams in High Asia, Earth Surface Processes and Landforms, 44(3), 808–824, https://doi.org/10.1002/esp.4532, 2019.

Bodin, X., Schoeneich, P., Deline, P., Ravanel, L., Magnin, F., Krysiecki, J.-M., and Echelard, T.: Le permafrost de montagne et les processus géomorphologiques associés: Évolutions récentes dans les Alpes françaises, Journal of Alpine Research | Revue de géographie alpine, 103–2, https://doi.org/10.4000/rga.2806, 2015.

https://doi.org/10.5194/egusphere-2025-117
Preprint. Discussion started: 20 February 2025

Bolch, T., and Marchenko, S.: Significance of glaciers, rockglaciers and ice-rich permafrost in the Northern Tien Shan as water towers under climate change conditions, IHP/HWRP-Berichte, 8, Article 8, https://doi.org/10.5167/uzh-137250, 2009.

Brahney, J., Clague, J. J., Edwards, T. W. D., and Menounos, B.: Late Holocene paleohydrology of Kluane Lake, Yukon Territory, Canada, Journal of Paleolimnology, 44(3), 873–885, https://doi.org/10.1007/s10933-010-9459-8, 2010.

Briggs, M. A., Hare, D. K., Boutt, D. F., Davenport, G., and Lane, J. W.: Thermal infrared video details multiscale groundwater discharge to surface water through macropores and peat pipes, Hydrological Processes, 30(14), 2510–2511, https://doi.org/10.1002/hyp.10722, 2016.

Brighenti, S., Engel, M., Dinale, R., Tirler, W., Voto, G., and Comiti, F.: Isotopic and chemical signatures of high mountain rivers in catchments with contrasting glacier and rock glacier cover, Journal of Hydrology, 623, https://doi.org/10.1016/j.jhydrol.2023.129779, 2023.

Brighenti, S., Tolotti, M., Bruno, M. C., Engel, M., Wharton, G., Cerasino, L., Mair, V., and Bertoldi, W.: After the peak water: The increasing influence of rock glaciers on alpine river systems, Hydrological Processes, 33(21), 2804–2823, https://doi.org/10.1002/hyp.13533, 2019.

Brunner, P., Therrien, R., Renard, P., Simmons, C. T., and Franssen, H.-J. H.: Advances in understanding river-groundwater interactions, Reviews of Geophysics, 55(3), 818–854, https://doi.org/10.1002/2017RG000556, 2017.

Carrivick, J. L., and Heckmann, T.: Short-term geomorphological evolution of proglacial systems, Geomorphology, 287, 3–28, https://doi.org/10.1016/j.geomorph.2017.01.037, 2017.

Carturan, L., Zuecco, G., Andreotti, A., Boaga, J., Morino, C., Pavoni, M., Seppi, R., Tolotti, M., Zanoner, T., and Zumiani, M.: Spring-water temperature suggests widespread occurrence of Alpine permafrost in pseudo-relict rock glaciers, EGUsphere, 1–35, https://doi.org/10.5194/egusphere-2023-2689, 2024.

Cartwright, I., and Hofmann, H.: Using radon to understand parafluvial flows and the changing locations of groundwater inflows in the Avon River, southeast Australia, Hydrology and Earth System Sciences, 20(9), 3581–3600, https://doi.org/10.5194/hess-20-3581-2016, 2016.

Casas-Mulet, R., Pander, J., Ryu, D., Stewardson, M. J., and Geist, J.: Unmanned Aerial Vehicle (UAV)-Based Thermal Infra-Red (TIR) and Optical Imagery Reveals Multi-Spatial Scale Controls of Cold-Water Areas Over a Groundwater-Dominated Riverscape, Frontiers in Environmental Science, 8, https://doi.org/10.3389/fenvs.2020.00064, 2020.

Chakravarti, P., Jain, V., and Mishra, V.: The distribution and hydrological significance of intact rock glaciers in the north-west Himalaya, Geografiska Annaler, Series A: Physical Geography, 104(3), 226–244, https://doi.org/10.1080/04353676.2022.2120262, 2022.

https://doi.org/10.5194/egusphere-2025-117
Preprint. Discussion started: 20 February 2025

Charonnat, B. and Baraer, M.: Supplemental Material: Drone-Based Thermal Infrared Imagery for Detection of Cold Groundwater Exfiltration in Shár Shaw Tagà, Yukon, Canada, Borealis, V1, https://doi.org/10.5683/SP3/O57OMY, 2025.

Chesnokova, A., Baraer, M., and Bouchard, É.: Proglacial icings as records of winter hydrological processes, The Cryosphere, 14(11), 4145–4164, https://doi.org/10.5194/tc-14-4145-2020, 2020.

Clow, D. W., Striegl, R. G., and Dornblaser, M. M.: Spatiotemporal Dynamics of CO2 Gas Exchange From Headwater Mountain Streams, Journal of Geophysical Research: Biogeosciences, 126(9), https://doi.org/10.1029/2021JG006509, 2021.

Colombo, N., Ferronato, C., Vittori Antisari, L., Marziali, L., Salerno, F., Fratianni, S., D'Amico, M. E., Ribolini, A., Godone, D., Sartini, S., Paro, L., Morra di Cella, U., and Freppaz, M.: A rock-glacier – pond system (NW Italian Alps): Soil and sediment properties, geochemistry, and trace-metal bioavailability, Catena, 194, https://doi.org/10.1016/j.catena.2020.104700, 2020.

Colombo, N., Gruber, S., Martin, M., Malandrino, M., Magnani, A., Godone, D., Freppaz, M., Fratianni, S., and Salerno, F.: Rainfall as primary driver of discharge and solute export from rock glaciers: The Col d'Olen Rock Glacier in the NW Italian Alps, Science of the Total Environment, 639, 316–330, https://doi.org/10.1016/j.scitotenv.2018.05.098, 2018.

Colombo, N., Salerno, F., Martin, M., Malandrino, M., Giardino, M., Serra, E., Godone, D., Said-Pullicino, D., Fratianni, S., Paro, L., Tartari, G., and Freppaz, M.: Influence of permafrost, rock and ice glaciers on chemistry of high-elevation ponds (NW Italian Alps), Science of the Total Environment, 685, 886–901, https://doi.org/10.1016/j.scitotenv.2019.06.233, 2019.

Colucci, R. R., Forte, E., Žebre, M., Maset, E., Zanettini, C., and Guglielmin, M. Is that a relict rock glacier? Geomorphology, 330, 177–189, https://doi.org/10.1016/j.geomorph.2019.02.002, 2019.

Croce, F., and Milana, J.: Internal structure and behavior of a Rock Glacier in the arid Andes of Argentina, Permafrost and Periglacial Processes, 13, 289–299, https://doi.org/10.1002/ppp.431, 2002.

Del Siro, C., Scapozza, C., Perga, M.-E., & Lambiel, C.: Investigating the origin of solutes in rock glacier springs in the Swiss Alps: A conceptual model, Frontiers in Earth Science, 11, https://doi.org/10.3389/feart.2023.1056305, 2023.

Delaloye, R., Lambiel, C., and Gärtner-Roer, I.: Overview of rock glacier kinematics research in the Swiss Alps: Seasonal rhythm, interannual variations and trends over several decades, Geographica Helvetica, 65(2), 135–145, https://doi.org/10.5194/gh-65-135-2010, 2010.

Dodds, C.J., and Campbell, R.B.: Overview, legend and mineral deposit tabulations for: GSC Open File 2188 to Open File 2191, Geological Survey of Canada, Energy Mines and Resources Canada, 85 p. + 5 maps, 1992.

https://doi.org/10.5194/egusphere-2025-117
Preprint. Discussion started: 20 February 2025

Engel, M., Penna, D., Bertoldi, G., Vignoli, G., Tirler, W., and Comiti, F.: Controls on spatial and temporal variability in streamflow and hydrochemistry in a glacierized catchment, Hydrology and Earth System Sciences, 23(4), 2041–2063, https://doi.org/10.5194/hess-23-2041-2019, 2019.

Ensom, T., Makarieva, O., Morse, P., Kane, D., Alekseev, V., and Marsh, P.: The distribution and dynamics of aufeis in permafrost regions, Permafrost and Periglacial Processes, 31(3), 383–395, https://doi.org/10.1002/ppp.2051, 2020.

Evin, M., Fabre, D., and Johnson, P. G.: Electrical Resistivity Measurements on the Rock Glaciers of Grizzly Creek, St Elias Mountains, Yukon, Permafrost and Periglacial Processes, 8, 11, 1997.

Falatkova, K., Šobr, M., Slavík, M., Bruthans, J., and Janský, B.: Hydrological characterization and connectivity of proglacial lakes to a stream, Adygine ice-debris complex, northern Tien Shan, Hydrological Sciences Journal, 65(4), 610–623, https://doi.org/10.1080/02626667.2020.1711913, 2020.

Frauenfelder, R., Allgöwer, B., Haeberli, W., and Hoelzle, M.: Permafrost investigations with GIS – a case study in the Fletschhorn area, Wallis,SwissAlps, InPermafrost, Proceedings of the Seventh International Conference, 23–27June 1998, Yellowknife, Canada, Lewkowicz AG, Allard M (eds) eds, Collection Nordicana 57, Centre d'études Nordiques, Université Laval: Québec; 291–295, 1998.

Gammons, C. H., Doolittle, M. F., Eastman, K. A., and Poulson, S. R.: Geochemistry of natural acid rock drainage in the Mt Evans area, Anaconda–Pintler Range, Montana, USA, Geochemistry: Exploration, Environment, Analysis, 21(4), https://doi.org/10.1144/geochem2021-068, 2021.

Haeberli, W.: Untersuchungen zur Verbreitung von Permafrost zwischen Flüelapass und Piz Grialetsch (Graubünden), Mitteilungen der VAW – ETH Zürich 17: 1–221, 1975.

Halla, C., Henrik Blöthe, J., Tapia Baldis, C., Trombotto Liaudat, D., Hilbich, C., Hauck, C., and Schrott, L.: Ice content and interannual water storage changes of an active rock glacier in the dry Andes of Argentina, Cryosphere, 15(2), 1187–1213, https://doi.org/10.5194/tc-15-1187-2021, 2021.

Harrington, J. S., Mozil, A., Hayashi, M., and Bentley, L. R.: Groundwater flow and storage processes in an inactive rock glacier, Hydrological Processes, 32(20), 3070–3088, https://doi.org/10.1002/hyp.13248, 2018.

Harrison, S., Jones, D., Anderson, K., Shannon, S., and Betts, R. A.: Is ice in the Himalayas more resilient to climate change than we thought? Geografiska Annaler, Series A: Physical Geography, 103(1), 1–7, https://doi.org/10.1080/04353676.2021.1888202, 2021.

Hayashi, M.: Alpine Hydrogeology: The Critical Role of Groundwater in Sourcing the Headwaters of the World. Groundwater, 58(4), 498–510, https://doi.org/10.1111/gwat.12965, 2020.

Hewitt, K.: Rock Glaciers and Related Phenomena. In K. Hewitt (Ed.), Glaciers of the Karakoram Himalaya: Glacial Environments, Processes, Hazards and Resources (pp. 267–289), Springer Netherlands, https://doi.org/10.1007/978-94-007-6311-1_11, 2014.

https://doi.org/10.5194/egusphere-2025-117
Preprint. Discussion started: 20 February 2025

Hock, R., Rasul, G., Adler, C., Cáceres, B., Gruber, S., Hirabayashi, Y., Jackson, M., Kääb, A., Kang, S., Kutuzov, S., Milner, Al., Molau, U., Morin, S., Orlove, B., and Steltzer, H.: High Mountain Areas. In: IPCC Special Report on the Ocean and Cryosphere in a Changing Climate [Pörtner, H.-O., Roberts, D.C., Masson-Delmotte, V., Zhai, P., Tignor, M., Poloczanska, E., Mintenbeck, K., Alegría, A., Nicolai, M., Okem, A., Petzold, J., Rama, B. and Weyer N.M. (eds.)]: Cambridge University Press, Cambridge, UK and New York, NY, USA, pp. 131-202, https://doi.org/10.1017/9781009157964.004, 2019.

Huss, M., Bookhagen, B., Huggel, C., Jacobsen, D., Bradley, R. S., Clague, J. J., Vuille, M., Buytaert, W., Cayan, D. r., Greenwood, G., Mark, B. g., Milner, A. M., Weingartner, R., and Winder, M.: Toward mountains without permanent snow and ice, Earth's Future, 5(5), 418–435, https://doi.org/10.1002/2016EF000514, 2017.

Iwasaki, K., Fukushima, K., Nagasaka, Y., Ishiyama, N., Sakai, M., and Nagasaka, A.: Real-Time Monitoring and Postprocessing of Thermal Infrared Video Images for Sampling and Mapping Groundwater Discharge, Water Resources Research, 59(4), e2022WR033630, https://doi.org/10.1029/2022WR033630, 2023.

Johnson, P. G.: Holocene Paleohydrology of the St. Elias Mountains, British Columbia and Yukon, Géographie Physique et Quaternaire, 40(1), 47–53, https://doi.org/10.7202/032622ar, 1986.

Johnson, P. G.: Mass Movement of Ablation Complexes and Their Relationship to Rock Glaciers, Geografiska Annaler, Series A, Physical Geography, 56(1/2), 93–101, https://doi.org/10.2307/520430, 1974.

Johnson, P. G.: Rock glacier types and their drainage systems, Grizzly Creek, Yukon Territory, Canadian Journal of Earth Sciences, 15(9), 1496–1507, https://doi.org/10.1139/e78-155, 1978.

Johnson, P. G.: Glacier-Rock Glacier Transition in the Southwest Yukon Territory, Canada, Arctic and Alpine Research, 12(2), 195, https://doi.org/10.2307/1550516, 1980.

Johnson, P. G.: Rock Glaciers, A Case for a Change in Nomenclature, Geografiska Annaler, Series A, Physical Geography, 65(1/2), 27–34, https://doi.org/10.2307/520718, 1983.

Johnson, P. G.: Stagnant Glacier Ice, St. Elias Mountains, Yukon, Geografiska Annaler, Series A, Physical Geography, 74(1), 13–19, https://doi.org/10.2307/521466, 1992.

Jones, D. B., Harrison, S., Anderson, K., and Betts, R. A.: Mountain rock glaciers contain globally significant water stores, Scientific Reports, 8(1), Article 1, https://doi.org/10.1038/s41598-018-21244-w, 2018.

Jones, D. B., Harrison, S., Anderson, K., Shannon, S., and Betts, R. A.: Rock glaciers represent hidden water stores in the Himalaya, Science of The Total Environment, 793, 145368, https://doi.org/10.1016/j.scitotenv.2021.145368, 2021.

Jones, D. B., Harrison, S., Anderson, K., and Whalley, W. B.: Rock glaciers and mountain hydrology: A review, Earth-Science Reviews, 193, 66–90, https://doi.org/10.1016/j.earscirev.2019.04.001, 2019.

Kalbus, E., Reinstorf, F., and Schirmer, M.: Measuring methods for groundwater and surface water interactions: review, Hydrology and Earth System Sciences, 10(6), 873–887, https://doi.org/10.5194/hess-10-873-2006, 2006.

https://doi.org/10.5194/egusphere-2025-117
Preprint. Discussion started: 20 February 2025

Käser, D., and Hunkeler, D.: Contribution of alluvial groundwater to the outflow of mountainous catchments, Water Resources Research, 52(2), 680–697, https://doi.org/10.1002/2014WR016730, 2016.

Krainer, K., and Mostler, W.: Hydrology of Active Rock Glaciers: Examples from the Austrian Alps, Arctic, Antarctic, and Alpine Research, 34(2), 142–149, https://doi.org/10.1080/15230430.2002.12003478, 2002.

Krainer, K., Mostler, W., and Spötl, C.: Discharge from active rock glaciers, Austrian Alps: A stable isotope approach, Austrian Journal of Earth Sciences, 100, 102–112, 2007.

Kummert, M., Bodin, X., Braillard, L., and Delaloye, R.: Pluri-decadal evolution of rock glaciers surface velocity and its impact on sediment export rates towards high alpine torrents, Earth Surface Processes and Landforms, 46(15), 3213–3227, https://doi.org/10.1002/esp.5231, 2021.

Liu, W., Fortier, R., Molson, J., and Lemieux, J.: A conceptual model for talik dynamics and icing formation in a river floodplain in the continuous permafrost zone at Salluit, Nunavik (Quebec), Canada, Permafrost and Periglacial Processes, 32(3), 468–483, https://doi.org/10.1002/ppp.2111, 2021.

Lloyd, S.: Least squares quantization in PCM, IEEE Transactions on Information Theory, 28(2), 129–137, IEEE Transactions on Information Theory, https://doi.org/10.1109/TIT.1982.1056489, 1982.

MacQueen, J.: Some methods for classification and analysis of multivariate observations, In Proceedings of the fifth Berkeley symposium on mathematical statistics and probability (Vol. 1, No. 14, pp. 281-297), 1967.

Mallinson, L., Swift, D. A., and Sole, A.: Proglacial icings as indicators of glacier thermal regime: Ice thickness changes and icing occurrence in Svalbard, Geografiska Annaler, Series A: Physical Geography, 101(4), 334–349, https://doi.org/10.1080/04353676.2019.1670952, 2019.

Marcer, M., Cicoira, A., Cusicanqui, D., Bodin, X., Echelard, T., Obregon, R., and Schoeneich, P.: Rock glaciers throughout the French Alps accelerated and destabilised since 1990 as air temperatures increased, Communications Earth & Environment, 2(1), 1–11, https://doi.org/10.1038/s43247-021-00150-6, 2021.

Marren, P. M., and Toomath, S. C.: Channel pattern of proglacial rivers: Topographic forcing due to glacier retreat, Earth Surface Processes and Landforms, 39(7), 943–951, https://doi.org/10.1002/esp.3545, 2014.

Müller, T., Lane, S. N., and Schaefli, B.: Towards a hydrogeomorphological understanding of proglacial catchments: An assessment of groundwater storage and release in an Alpine catchment, Hydrology and Earth System Sciences, 26(23), 6029–6054, https://doi.org/10.5194/hess-26-6029-2022, 2022.

Müller, T., Roncoroni, M., Mancini, D., Lane, S. N., and Schaefli, B.: Current and future roles of meltwater–groundwater dynamics in a proglacial Alpine outwash plain, Hydrology and Earth System Sciences, 28(4), 735–759, https://doi.org/10.5194/hess-28-735-2024, 2024.

Navarro, G., Valois, R., MacDonell, S., de Pasquale, G., and Díaz, J. P.: Internal structure and water routing of an ice-debris landform assemblage using multiple geophysical methods in the semiarid Andes, Frontiers in Earth Science, 11, https://doi.org/10.3389/feart.2023.1102620, 2023.

https://doi.org/10.5194/egusphere-2025-117
Preprint. Discussion started: 20 February 2025

PERMOS Report 2019-16-19 | PERMOS – Swiss Permafrost Monitorinig Network, Retrieved 17 September 2024, from https://www.permos.ch/doi/permos-rep-2019-16-19, 2019.

Porter, C., Howat, I., Noh, M.-J., Husby, E., Khuvis, S., Danish, E., Tomko, K., Gardiner, J., Negrete, A., Yadav, B., Klassen, J., Kelleher, C., Cloutier, M., Bakker, J., Enos, J., Arnold, G., Bauer, G., and Morin, P.: ArcticDEM - Mosaics, Version 4.1 [Dataset], Harvard Dataverse, https://doi.org/10.7910/DVN/3VDC4W, 2023.

Rautio, A., Kivimäki, A.-L., Korkka-Niemi, K., Nygård, M., Salonen, V.-P., Lahti, K., and Vahtera, H.: Vulnerability of groundwater resources to interaction with river water in a boreal catchment, Hydrology and Earth System Sciences, 19(7), 3015–3032, https://doi.org/10.5194/hess-19-3015-2015, 2015.

Reato, A., Borzi, G., Martínez, O. A., and Carol, E.: Role of rock glaciers and other high-altitude depositional units in the hydrology of the mountain watersheds of the Northern Patagonian Andes, Science of The Total Environment, 824, 153968, https://doi.org/10.1016/j.scitotenv.2022.153968, 2022.

Robinson, C. T., Jolidon, C., Consoli, G., Bloem, S., and Ebi, C.: Temporal dynamics in the physico-chemistry of a high-alpine stream network in the Swiss National Park, Eco.Mont, 14(2), 11–23, https://doi.org/10.1553/eco.mont-14-2s11, 2022.

Scapozza, C.: Contributo dei metodi termici alla prospezione del permafrost montano: esempi dal massiccio della Cima di Gana Bianca (Val Blenio, Svizzera), Bollettino della Società Ticinese di Scienze Naturali 97:55–66, 2009.

Scapozza, C.: Investigation on protalus ramparts in the Swiss Alps, Geographica Helvetica, 70(2), 135–139, https://doi.org/10.5194/gh-70-135-2015, 2015.

Schreder, S., Sommaruga, R., Psenner, R., Chimani, B., Ganekind, M., and Koinig, K. A.: Changes in air temperature, but not in precipitation, determine long-term trends in water chemistry of high mountain lakes of the Alps with and without rock glacier influence, Science of the Total Environment, 905, https://doi.org/10.1016/j.scitotenv.2023.167750, 2023.

Scotti, R., Crosta, G. B., and Villa, A.: Destabilisation of Creeping Permafrost: The Plator Rock Glacier Case Study (Central Italian Alps), Permafrost and Periglacial Processes, 28(1), 224–236, https://doi.org/10.1002/ppp.1917, 2017.

Sorg, A., Kääb, A., Roesch, A., Bigler, C., and Stoffel, M.: Contrasting responses of Central Asian rock glaciers to global warming, Scientific Reports, 5, https://doi.org/10.1038/srep08228, 2015.

Terry, N., Grunewald, E., Briggs, M., Gooseff, M., Huryn, A. D., Kass, M. A., Tape, K. D., Hendrickson, P., and Lane, J. W., Jr.: Seasonal Subsurface Thaw Dynamics of an Aufeis Feature Inferred From Geophysical Methods, Journal of Geophysical Research: Earth Surface, 125(3), https://doi.org/10.1029/2019JF005345, 2020.

Tjoelker, A., Baraer, M., Valence, E., Charonnat, B., Masse-Dufresne, J., Mark, B., and McKenzie, J.: Drone-Based Ground-Penetrating Radar with Manual Transects for Improved Field Surveys of Buried Ice, Remote Sensing, 16, 2461, https://doi.org/10.3390/rs16132461, 2024.

https://doi.org/10.5194/egusphere-2025-117
Preprint. Discussion started: 20 February 2025

Toran, L.: Groundwater–Surface Water Interaction, In Encyclopedia of Water (pp. 1–12), John Wiley & Sons, Ltd, https://doi.org/10.1002/9781119300762.wsts0027, 2019.

Tronstad, L. M., Hotaling, S., Giersch, J. J., Wilmot, O. J., and Finn, D. S.: Headwaters Fed by Subterranean Ice: Potential Climate Refugia for Mountain Stream Communities? Western North American Naturalist, 80(3), 395–407, https://doi.org/10.3398/064.080.0311, 2020.

van Tiel, M., Aubry-Wake, C., Somers, L., Andermann, C., Avanzi, F., Baraer, M., Chiogna, G., Daigre, C., Das, S., Drenkhan, F., Farinotti, D., Fyffe, C. L., de Graaf, I., Hanus, S., Immerzeel, W., Koch, F., McKenzie, J. M., Müller, T., Popp, A. L., … Yapiyev, V.: Cryosphere–groundwater connectivity is a missing link in the mountain water cycle, Nature Water, 2(7), 624–637, https://doi.org/10.1038/s44221-024-00277-8, 2024.

Vélez-Nicolás, M., García-López, S., Barbero, L., Ruiz-Ortiz, V., and Sánchez-Bellón, Á.: Applications of Unmanned Aerial Systems (UASs) in Hydrology: A Review, Remote Sensing, 13(7), Article 7, https://doi.org/10.3390/rs13071359, 2021.

Wagner, T., Brodacz, A., Krainer, K., and Winkler, G.: Active rock glaciers as shallow groundwater reservoirs, Austrian Alps, Grundwasser, 25(3), 215–230, https://doi.org/10.1007/s00767-020-00455-x, 2020.

Wagner, T., Kainz, S., Krainer, K., and Winkler, G.: Storage-discharge characteristics of an active rock glacier catchment in the Innere Ölgrube, Austrian Alps, Hydrological Processes, 35(5), https://doi.org/10.1002/hyp.14210, 2021.

Wagner, T., Pauritsch, M., and Winkler, G.: Impact of relict rock glaciers on spring and stream flow of alpine watersheds: Examples of the Niedere Tauern Range, Eastern Alps (Austria), Austrian Journal of Earth Sciences, 109(1), https://doi.org/10.17738/ajes.2016.0006, 2016.

Wainstein, P., Moorman, B., and Whitehead, K.: Glacial conditions that contribute to the regeneration of Fountain Glacier proglacial icing, Bylot Island, Canada, Hydrological Processes, 28(5), 2749–2760, https://doi.org/10.1002/hyp.9787, 2014.

Wanner, C., Moradi, H., Ingold, P., Cardenas Bocanegra, M. A., Mercurio, R., and Furrer, G.: Rock glaciers in the Central Eastern Alps – How permafrost degradation can cause acid rock drainage, mobilization of toxic elements and formation of basaluminite, Global and Planetary Change, 227, https://doi.org/10.1016/j.gloplacha.2023.104180, 2023.

Webb, B. W., Hannah, D. M., Moore, R. D., Brown, L. E., and Nobilis, F.: Recent advances in stream and river temperature research, Hydrological Processes, 22(7), 902–918, https://doi.org/10.1002/hyp.6994, 2008.

Winkler, G., Wagner, T., Pauritsch, M., and Kellerer-Pirklbauer, A.: What will occur after permafrost? Relevance of relict rock glaciers for the discharge behaviour of alpine catchments, Joannea - Geologie und Palaontologie, 12, 63–72, 2016.

https://doi.org/10.5194/egusphere-2025-117
Preprint. Discussion started: 20 February 2025

Zarroca, M., Roqué, C., Linares, R., Salminci, J. G., and Gutiérrez, F.: Natural acid rock drainage in alpine catchments: A side effect of climate warming, Science of The Total Environment, 778, 146070, https://doi.org/10.1016/j.scitotenv.2021.146070, 2021.

Zierl, B., and Bugmann, H.: Global change impacts on hydrological processes in Alpine catchments, Water Resources Research, 41(2), https://doi.org/10.1029/2004WR003447, 2005.